Molecular Plant
Research Article

CellPress
PARTNER JOURNAL

Producing Designer Oils in Industrial Microalgae by Rational Modulation of Co-evolving Type-2 Diacylglycerol Acyltransferases

Yi Xin[1,7,8], Yandu Lu[1,7,8], Yi-Ying Lee[2,8], Li Wei[1,7], Jing Jia[1,7], Qintao Wang[1,7], Dongmei Wang[1,7], Fali Bai[6,7], Hanhua Hu[5,7], Qiang Hu[4,7], Jin Liu[2,3,*], Yantao Li[2,*] and Jian Xu[1,7,*]

[1]Single-Cell Center, CAS Key Laboratory of Biofuels and Shandong Laboratory of Energy Genetics, Qingdao Institute of BioEnergy and Bioprocess Technology, Chinese Academy of Sciences, Qingdao, Shandong 266101, China

[2]Institute of Marine and Environmental Technology, University of Maryland Center for Environmental Science and University of Maryland, Baltimore County, Baltimore, MD 21202, USA

[3]Institute for Food and Bioresource Engineering and Department of Energy and Resource Engineering, College of Engineering, Peking University, Beijing 100871, China

[4]Center for Microalgal Biotechnology and Biofuels, Institute of Hydrobiology, Chinese Academy of Sciences, Wuhan, Hubei 430072, China

[5]Diatom Biology Group, Institute of Hydrobiology, Chinese Academy of Sciences, Wuhan, Hubei 430072, China

[6]Core Laboratory, Qingdao Institute of BioEnergy and Bioprocess Technology, Chinese Academy of Sciences, Qingdao, Shandong 266101, China

[7]University of Chinese Academy of Sciences, Beijing 100049, China

[8]These authors contributed equally to this article.

***Correspondence: Jin Liu (gjinliu@pku.edu.cn), Yantao Li (yantao@umces.edu), Jian Xu (xujian@qibebt.ac.cn)**

https://doi.org/10.1016/j.molp.2017.10.011

ABSTRACT

Microalgal oils, depending on their degree of unsaturation, can be utilized as either nutritional supplements or fuels; thus, a feedstock with genetically designed and tunable degree of unsaturation is desirable to maximize process efficiency and product versatility. Systematic profiling of *ex vivo* (in yeast), *in vitro*, and *in vivo* activities of type-2 diacylglycerol acyltransferases in *Nannochloropsis oceanica* (NoDGAT2s or NoDGTTs), via reverse genetics, revealed that NoDGAT2A prefers saturated fatty acids (SFAs), NoDGAT2D prefers monounsaturated fatty acids (MUFAs), and NoDGAT2C exhibits the strongest activity toward polyunsaturated fatty acids (PUFAs). As *NoDGAT2A*, *2C*, and *2D* originated from the green alga, red alga, and eukaryotic host ancestral participants of secondary endosymbiosis, respectively, a mechanistic model of oleaginousness was unveiled, in which the indigenous and adopted *NoDGAT2s* formulated functional complementarity and specific transcript abundance ratio that underlie a rigid SFA:MUFA:PUFA hierarchy in triacylglycerol (TAG). By rationally modulating the ratio of *NoDGAT2A*:*2C*:*2D* transcripts, a bank of *N. oceanica* strains optimized for nutritional supplement or fuel production with a wide range of degree of unsaturation were created, in which proportion of SFAs, MUFAs, and PUFAs in TAG varied by 1.3-, 3.7-, and 11.2-fold, respectively. This established a novel strategy to simultaneously improve productivity and quality of oils from industrial microalgae.

Key words: biofuels, degree of unsaturation, genetic engineering, diacylglycerol acyltransferase, *Nannochloropsis*

Xin Y., Lu Y., Lee Y.-Y., Wei L., Jia J., Wang Q., Wang D., Bai F., Hu H., Hu Q., Liu J., Li Y., and Xu J. (2017). Producing Designer Oils in Industrial Microalgae by Rational Modulation of Co-evolving Type-2 Diacylglycerol Acyltransferases. Mol. Plant. **10**, 1523–1539.

INTRODUCTION

The high photosynthetic growth potential and rich oil content of many oleaginous microalgae has led to growing interest in utilizing their biomass as feedstock for scalable production of biofuels and biomaterials from carbon dioxide (Hu et al., 2008; Wijffels and Barbosa, 2010; Georgianna and Mayfield, 2012). Triacylglycerol (TAG) is a main form of energy storage in microalgal cells and can represent as much as 60% of cell dry weight (Hu et al., 2008). Each TAG molecule consists of three fatty acid (FA)

Published by the Molecular Plant Shanghai Editorial Office in association with Cell Press, an imprint of Elsevier Inc., on behalf of CSPB and IPPE, SIBS, CAS.

moieties that are anchored to a glycerol scaffold. Depending on the degree of unsaturation (DU), each fatty acid molecule can be classified as a saturated FA (SFA), a monounsaturated FA (MUFA), or a polyunsaturated FA (PUFA). Hence, diversity and relative abundance of these TAG-associated SFAs, MUFAs, and PUFAs decide the overall DU of the TAG molecules, which is a key property in determining the application area, economical value, and market potential of microalgal oil products. For example, biodiesel converted from FAs of low DU produce biodiesel with superior oxidative stability yet rather poor low-temperature properties, whereas biodiesel converted from FAs with high DU has good cold-flow properties yet is particularly susceptible to oxidation (Knothe, 2008); thus, FAs with high MUFAs are globally suitable as transportation fuel (Ramos et al., 2009). On the other hand, FAs with high DU, i.e., those rich in PUFAs such as eicosapentaenoic acid (EPA) and docosahexaenoic acid (DHA), can serve as high-value nutrient supplements with well-documented health benefits to humans. Since human and animals are not able to synthesize EPA and DHA, adequate intakes from external sources, usually microalgae, are required (Kwak et al., 2012).

In light of such diversity and versatility in the FA products, a microalgal feedstock capable of producing TAGs with rationally designed and genetically encoded FA-DU is highly desirable. Compared with the traditional approach whereby multiple microalgal species each with a distinct SFA:MUFA:PUFA profile are to be chosen from, a platform building on a bank of strains all derived from a single species, with each featuring a rationally designed and genetically specified SFA:MUFA:PUFA profile yet together covering a wide range of FA-DU, would negate the need to switch among various sets of cultivation and harvesting parameters or between distinct production modes. This can boost the efficiency and cost saving in production while enabling nimble response to the constantly changing market needs (Wang et al., 2011; Georgianna and Mayfield, 2012; Smanski et al., 2016).

In microalgal cells, TAG molecules are assembled from FAs by a class of enzymes universally found in plants and animals including diacylglycerol acyltransferases (DGATs). Surprisingly, despite their much smaller size, microalgal genomes harbor a gene dose of type-2 *DGAT*s (*DGAT2*s or *DGTT*s) that is often many times larger than higher plants and animals (Vieler et al., 2012; Wang et al., 2014). In addition, in industrial oleaginous microalgae such as *Nannochloropsis* spp., the vast array of *DGAT2s* transcripts is polyphyletic (Vieler et al., 2012; Wang et al., 2014) and exhibits highly distinct and temporally coordinated patterns during nitrogen-depletion-induced TAG biosynthesis (Li et al., 2014), which suggests active yet distinct functions *in vivo* among the co-evolving *DGAT2s*. Such functional differentiation is potentially linked to FA-DU, as for example, overexpression of an endogenous DGAT in the green alga *Neochloris oleoabundans* led to an increase of the SFA level in TAG to 58% and reduction of PUFAs in TAG to 9% (Klaitong et al., 2017). However, since the mechanism regulating assembly of SFAs, MUFAs, or PUFAs into TAGs *in vivo* remains largely unknown for industrial microalgae, a rational approach to generate feedstocks that produce TAGs with genetically designed FA-DU or designated ratio of SFAs/MUFAs/PUFAs has not yet been demonstrated.

In this study, targeting the industrial oleaginous microalga *Nannochloropsis oceanica*, which harbors the largest dose of type-2 *DGAT*s (11 *NoDGAT2*s) known to date, we reconstructed an *in vivo* model of TAG synthesis by systematically probing the *in silico*, *ex vivo* (i.e., enzyme activity profiling in yeast), *in vitro*, and *in vivo* functions of NoDGAT2s via reverse genetics and lipidomic approaches. Functional stratification of the NoDGAT2s was revealed, whereby NoDGAT2A prefers SFAs, 2D prefers MUFAs, and 2C exhibits the highest activity for PUFAs among the three NoDGAT2s. Furthermore, by modulating these *NoDGAT2s* via knockdown or overexpression, a bank of *N. oceanica* lines that optimized for nutritional supplements or fuel production or both with a wide range of FA-DU were established. Our findings unravel functional stratification in SFA/MUFA/PUFA preference among DGAT2s as a key mechanism of oleaginousness in industrial microalgae, and demonstrate that the genetic diversity, ratio of transcript abundance, and functional complementarity derived from secondary symbiosis can be exploited for rational design of oil property and simultaneous enhancement of oil productivity in industrial microalgae.

RESULTS

Distinct Ancestral Origins of *NoDGAT2*s Based on Validated Coding Sequences

Gene models of all candidate *DGAT2s* in the eustigmatophyte *N. oceanica* (strain IMET1) were validated by cDNA sequencing, revealing 11 full-length *DGAT2*s (*NoDGAT2A* to *NoDGAT2K*; Supplemental Table 1; Supplemental Dataset 1; Methods). They are of more compact gene structures than those from the green alga *Chlamydomonas reinhardtii* or the diatom *Phaeodactylum tricornutum*, as no more than five introns are present in each *NoDGAT2* (Supplemental Table 1 and Supplemental Figure 1A). *In silico* analysis revealed one to three transmembrane domains in each of them (except NoDGAT2G, which harbors seven transmembrane domains), consistent with type-2 DGATs in higher plants (Shockey et al., 2006) and other microalgae (Sanjaya et al., 2013) (Supplemental Table 1 and Supplemental Figure 1B; Methods). Interestingly, sequence identity among the 11 *NoDGAT2*s is relatively low, arguing against recent gene duplication (Flagel and Wendel, 2009) (Supplemental Table 2). Phylogenetic analysis of the type-2 DGATs from *N. oceanica* and other model organisms (including higher plants, green algae, red algae, and fungi) suggested that the 11 *NoDGAT2*s were derived from three distinct lineages that participated in the secondary endosymbiosis: green algae lineage (*2A*, *2B*, *2G*, *2I*, *2K*), red algae lineage (*2C*), and heterotrophic eukaryotic secondary host lineage (*2D*, *2E*, *2F*, *2H*, *2J*), respectively (Supplemental Figure 2), which is consistent with the evolution model based on predicted *NoDGAT2* sequences (Wang et al., 2014).

Expression of 11 *NoDGAT2*s Individually in a TAG-Deficient Yeast Reveals TAG-Synthetic Activity but Different Substrate Specificity of NoDGAT2A, 2C, and 2D

To probe their function, we expressed the coding sequence of each of the 11 *NoDGAT2*s in *Saccharomyces cerevisiae* strain H1246, a TAG-deficient quadruple knockout mutant (see

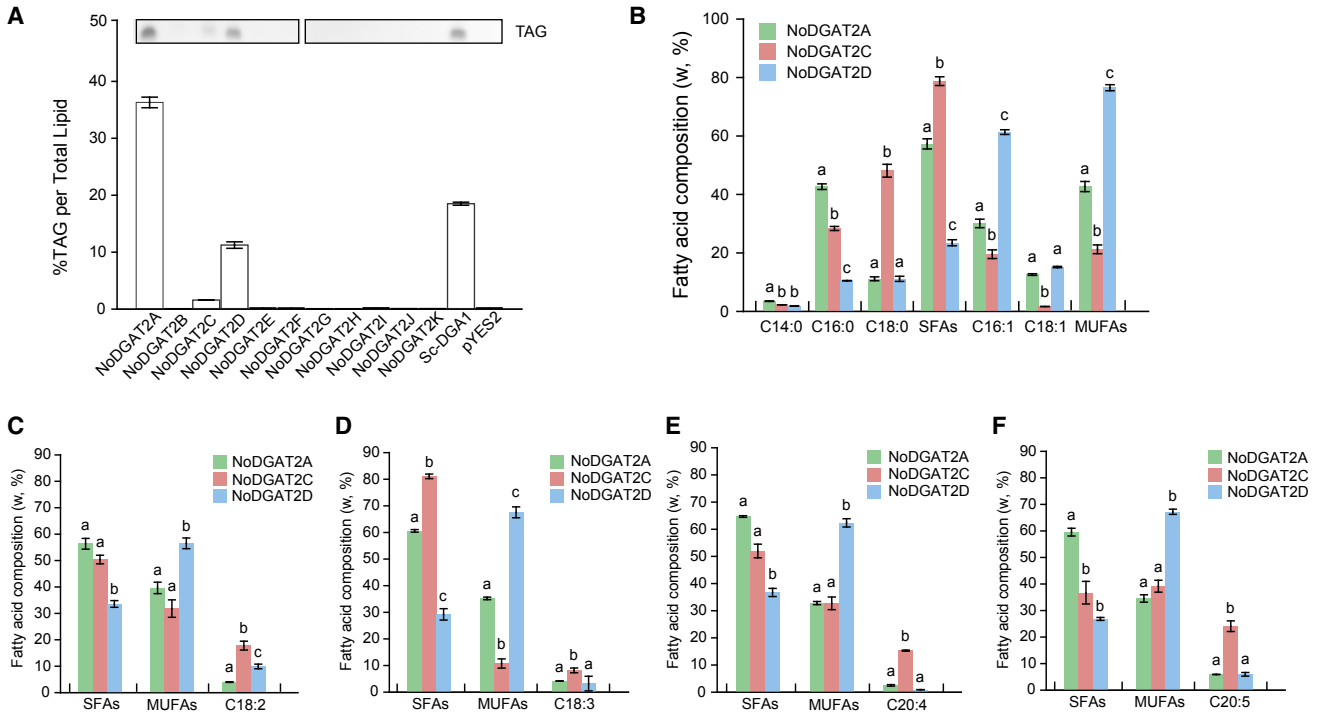

Figure 1. Complementation of the TAG-Deficient Phenotype in Mutant Yeast H1246 by Expression of *NoDGAT2*s.

(A) GC–MS quantification of TAG levels extracted from transformed yeast. The total amount of TAG was normalized based on that of the total lipids.

(B) Profiles of major FA derived from TAGs in the *NoDGAT2*-carrying yeasts.

(C–F) Profiles of major FAs derived from TAGs in the *NoDGAT2*-carrying yeasts after the feeding of C18:2 **(C)**, C18:3 **(D)**, C20:4 **(E)**, or C20:5 **(F)**. Values are presented as mean ± SD ($n = 3$). Different letters above the bars grouped by each acyl CoA indicate significant difference ($p \leq 0.05$), based on one-way analysis of variance (ANOVA) and Tukey's honestly significant difference (HSD) test.

Methods [Sandager et al., 2002]). TLC analysis of total lipids (TLs) revealed that TAG was undetectable in the yeasts carrying the empty vector, yet upon expression of three of the 11 genes, *NoDGAT2A*, *2C*, or *2D* (each from a distinct ancestral lineage; Supplemental Figure 2), a prominent spot corresponding to TAG appeared just like expression of an endogenous yeast *DGAT2* (*ScDGA1*) (Figure 1A). However, probably due to lack of DGAT activity (i.e., they might possess other enzymatic activities) or absence in yeast of proper substrates or co-factors for TAG synthesis, TAG was not detected in H1246 strains expressing the other *NoDGAT2s*, which were thus excluded from further characterization.

Gas chromatography–mass spectrometry (GC–MS) revealed that, as compared with the empty vector control (0.17% per TL), the *NoDGAT2A*-, *2C*-, and *2D*-carrying yeasts each accumulated a considerable level of TAG (36.31%, 1.59%, and 11.25% per TL, respectively), confirming their TAG-synthetic activity *ex vivo* (Figure 1A). In the TAG produced, five major FAs including three SFAs (C14:0, C16:0, and C18:0) and two MUFAs (C16:1 and C18:1) were identified (Figure 1B). However, among the yeast lines, dominant FA species in TAG were distinct: C16:0, C18:0, and C16:1 were the most abundant species (accounting for 42.7%, 48.1%, and 61.3% of total TAG-associated FA in each) in the *2A*-, *2C*-, and *2D*-carrying yeasts, respectively. Collectively H1246-*NoDGAT2C* accumulated much higher levels of SFAs than MUFAs (78.8% versus 21.2% per total FA); by contrast, the *2D*-carrying lines accumulated much higher levels of MUFAs than SFAs (23.5% versus 76.5%; Figure 1B). Thus acyl-coenzyme A (CoA) specificity among the *NoDGAT2s* appears distinct, in terms of both carbon chain length and DU.

Ex Vivo PUFA-Feeding Assay in Yeast Reveals Diverse Substrate Preference and Distinct TAG Product Profile among NoDGAT2A, 2C, and 2D

PUFA substrates such as linoleic acid (LA; C18:2, n9,12), linolenic acid (ALA; C18:3, n6,9,12), arachidonic acid (ARA; C20:4, n6,9,12,15), and EPA (C20:5, n5,8,11,14,17) were absent in the yeast H1246, yet are found in TAG of *N. oceanica* (Li et al., 2014). Thus to determine the PUFA preference of NoDGAT2A/2C/2D, the four PUFAs were individually fed to H1246 cells carrying the *NoDGAT2s* or *ScDGA1* (as positive control). While PUFA-fed *2A*-, *2D*-, and *ScDGA1*-carrying yeasts accumulated lower amounts of TAGs than unfed samples (probably due to toxicity of FAs), *2C*-carrying yeasts featured a much higher TAG level than the unfed control (1.6% per TL) upon feeding of C20:4 (4.1% per TL) or C20:5 (4.4% per TL; Supplemental Figure 3). Thus it appears that NoDGAT2C prefers the PUFAs of C20:4 and C20:5 as its substrates whereas 2A, 2D, and ScDGA1 have no such preference.

To further characterize such preference, we revealed the profiles of TAG-associated FAs after PUFA feeding. Similar to

observations in the absence of PUFA feeding, SFAs and MUFAs were the major FAs in the yeasts carrying *NoDGAT2A* and *2D*, respectively (Figure 1C–1F). On the other hand, TAGs in the *2C*-carrying yeasts harbor significantly more PUFAs than those in the *2A*- and *2D*-carrying yeasts, upon addition of C18:2 (17.8% in 2C versus 4.0% in 2A and 9.9% in 2D, Figure 1C), C18:3 (8.2% versus 4.2% and 3.2%, Figure 1D), C20:4 (15.3% versus 2.5% and 0.9%, Figure 1E), or C20:5 (24.09% versus 5.9% and 6.0%, Figure 1F). Therefore when SFAs, MUFAs, and PUFAs are all present, although *2A*-, *2C*-, and *2D*-carrying yeasts all can utilize each of the three substrate classes, 2A prefers SFAs, 2D prefers MUFAs, and 2C exhibits a stronger PUFA-incorporating activity than the other two NoDGAT2s.

To probe the product profiles of NoDGAT2s at the finer resolution of individual TAG species, we performed electrospray ionization mass spectrometry (ESI-MS) analysis for the H1246-*NoDGAT2* lines, either with or without the PUFA feeding (Supplemental Figure 4; Methods; H1246-*ScDGA1* as a control). A total of 77 major TAG species were identified, with TAG50:2 (16:0/16:1/18:1) accounting for the highest cellular content (17.09%–22.24%) in all H1246-*NoDGAT2A* samples. In H1246-*NoDGAT2C*, the most abundant TAG species were TAG52:3 (16:1/18:1/18:1) without PUFA feeding (18.1%), TAG52:3 (16:0/18:1/18:2) with C18:2 supply (7.8%), TAG54:4 (18:0/18:1/18:3) with C18:3 supply (10.4%), TAG54:6 (16:1/18:1/20:4) with supply of C20:4 (16.2%), and TAG54:7 (16:1/18:1/20:5) with supply of C20:5 (18.4%). In all H1246-*NoDGAT2D* samples supplemented with or without C18:2, C20:4, or C20:5, TAG50:3 (16:1/16:1/18:1) was the most abundant TAG species (14.0%–31.9%), yet TAG54:9 (18:3/18:3/18:3) topped the list (15.4%) in H1246-*NoDGAT2D* samples supplied with C18:3. Considering the low level of TAG/TL ratio and the high content of C18:3-TAGs in the *NoDGAT2C*- and *2D*-carrying yeasts (Supplemental Figure 3), it is possible that free C18:3 was aggressively incorporated into TAG to cope with the FA toxicity. Therefore, consistent with the GC–MS data, *NoDGAT2A*- and *2D*-carrying yeasts incorporated more SFAs and MUFAs into TAGs than *2C*, while *2C* exhibited a higher enzyme activity for PUFAs than the other two NoDGAT2s.

On the other hand, H1246-*NoDGAT2A* synthesized more TAG46 and TAG48 while less TAG56, TAG58, and TAG60 than H1246-*ScDGA1* under all the feeding conditions (Supplemental Figure 4). In contrast, H1246-*NoDGAT2C* produced less TAG46, TAG48, and TAG50 but more TAG52 and TAG54 than H1246-*ScDGA1* in the absence of supplements. Moreover, higher contents of TAG50, TAG52, TAG56, and TAG58 were detected in H1246-*NoDGAT2C* than in H1246-*ScDGA1* when C18:3, C20:4, or C20:5 were fed. Meanwhile, H1246-*NoDGAT2D* shows a product pattern similar to that of *2A*, as it contains more TAG46, TAG48, and TAG50 than H1246-*ScDGA1* under all feeding conditions. Thus, besides the SFA/MUFA/PUFA preference, ESI-MS revealed another layer of complementarity in carbon chain length of FA substrates, with 2A preferring SFA CoAs and shorter-chain (i.e., C14 and C16) acyl-CoAs/DAGs and 2C preferring PUFA CoAs and longer-chain (i.e., C18 and C20) acyl-CoAs/DAGs, yet 2D preferring MUFA CoAs and shorter-chain acyl-CoAs/DAGs.

In Vitro Enzymatic Assay Pinpointed Acyl-CoA and DAG Specificity of NoDGAT2s

To further validate the distinct substrate preference of NoDGAT2A, 2C, and 2D, we performed a non-radiolabeled *in vitro* DGAT assay to measure activity and substrate specificity of NoDGAT2s toward acyl-CoAs and DAGs (Liu et al., 2016a). Ten acyl-CoAs, including C16:0 CoA, C16:1 CoA, C18:0 CoA, C18:1 CoA, C18:2 CoA, C18:3n3 CoA, C18:3n6 CoA, C20:4 CoA, C20:5 CoA, and C22:6 CoA, were introduced to test substrate preference of NoDGAT2A, 2C, and 2D, with prokaryotic C18:1/C16:0 DAG (the most abundant DAG in *N. oceanica* IMET1 [Li et al., 2014]) as the acyl acceptor.

Results from the *in vitro* substrate feeding revealed that NoDGAT2A exhibited the highest TAG-synthetic activity toward C16:0 while among the C18 acyl-CoAs, C18:1 was preferred. Among monounsaturated ones 2A preferred shorter-chain acyl-CoA, as the C16:1 feeding resulted in more TAG than C18:1 (Figure 2A). NoDGAT2C, on the other hand, appeared to prefer MUFA over SFA and PUFA (Figure 2B). In contrast, NoDGAT2D showed the highest activity on C16:1 CoA (Figure 2C). NoDGAT2A exhibited a considerably higher activity on C16:0 CoA than NoDGAT2C and 2D (Figure 2D), suggesting NoDGAT2A as the major contributor among the tested NoDGAT2s for incorporating C16:0 into *sn*-3 position of DAG for TAG synthesis. NoDGAT2A and 2D had comparable enzymatic activity on C16:1 CoA, both higher than NoDGAT2C. As for C18:1 CoA, NoDGAT2C exhibited slightly higher activity than NoDGAT2A, while NoDGAT2D showed almost no activity. However, all three NoDGAT2s showed low or no activity on the PUFA CoAs *in vitro* (C18:2, C18:3, C20:4, C20:5, and C22:6 CoAs). These *in vitro* results combined with the *ex vivo* data (Figure 1B–1F) further support that among the three NoDGAT2s, 2A prefers SFA CoAs and 2D prefers MUFA CoAs. However, the PUFA preference of NoDGAT2C between *ex vivo* and *in vitro* results is inconsistent. Considering that the TAG-associated FA composition is ultimately determined by the availability of FAs in the host and its set of desaturases, deducing substrate specificity from yeast experiments has its own limitation. Therefore, clarification of this would require *in vivo* activity assay.

Furthermore, enzymatic activity and preference on DAGs, the other substrate of DGAT, was profiled. Eight DAGs were tested, including seven 1,2-DAGs (three prokaryotic [C16:0/C16:0, C16:1/C16:1, C18:1/16:0] and four eukaryotic [C16:0/C18:1, C18:1/C18:1, C18:2/18:2, C18:3/18:3]) and one 1,3-DAG (1,3-C18:1/C18:1). When using C16:0 CoA as the acyl donator, NoDGAT2A had slightly higher activity on C18:1/C16:0 than on C16:1/C16:1, C16:0/C18:1, and C18:1/C18:1 DAGs, while it showed weak activity on 1,3-C18:1/C18:1, C18:2/C18:2 and C18:3/C18:3 DAGs (Supplemental Figure 5A). When the acyl donor was C16:1 or C18:1 CoA, NoDGAT2A exhibited a moderately higher activity on C16:0/C18:1 and C18:1/C18:1 DAGs than on the other three tested prokaryotic DAGs. NoDGAT2C, unlike 2A, preferred the eukaryotic C16:0/C18:1 and C18:1/C18:1 DAGs over prokaryotic DAGs for TAG formation with all acyl-CoAs tested (Supplemental Figure 5B).

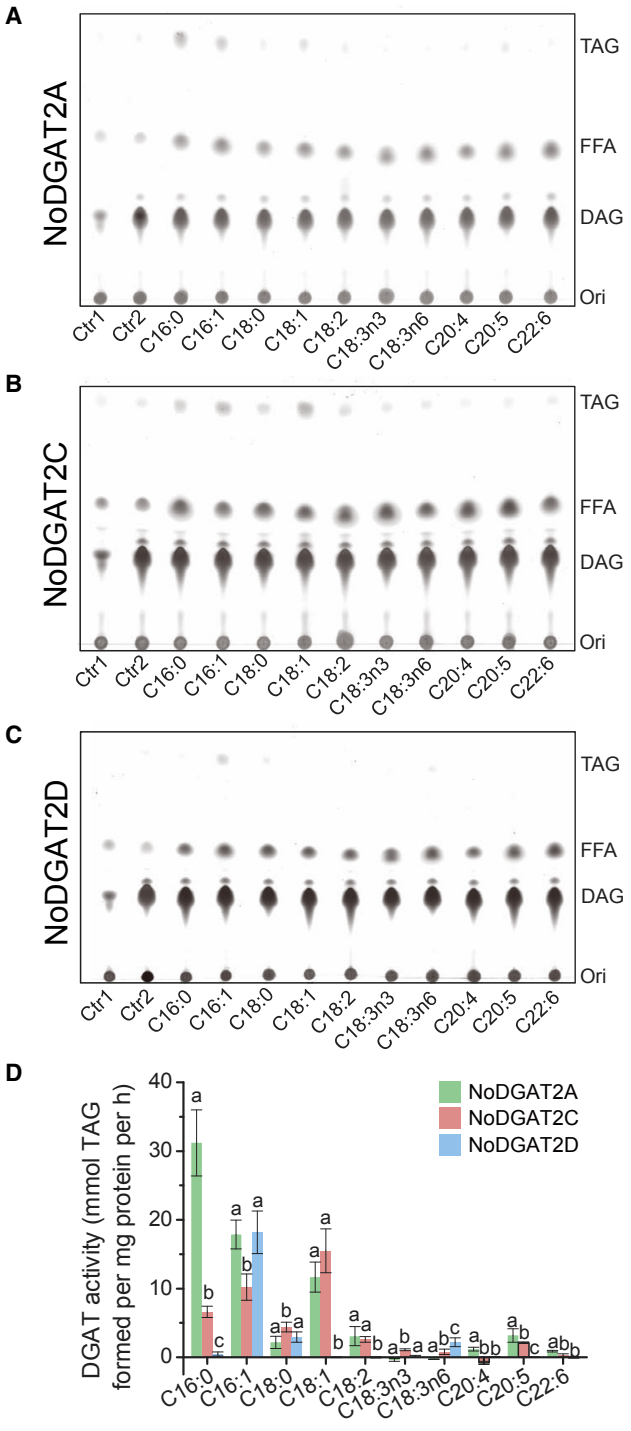

Figure 2. Substrate Specificities of NoDGAT2A, 2C, and 2D for Acyl-CoAs *In Vitro*.

(A–C) TLC analysis of lipids from *in vitro* enzymatic reactions of NoDGAT2A **(A)**, NoDGAT2C **(B)**, and NoDGAT2D **(C)** with various acyl-CoAs. C18:1/C16:0 DAG was used as the acyl acceptor. Experiments were conducted in triplicate, each with one representative TLC shown.

(D) Quantification of specific activity of NoDGAT2A, 2C, and 2D by GC–MS. Ctr1, microsome; Ctr2, microsome plus 250 μM DAG. Values are presented as mean ± SD ($n = 3$). Different letters above the bars grouped by each acyl-CoA indicate significant difference ($p \leq 0.05$), based on one-way analysis of variance and Tukey's honest significant difference test.

Similar to NoDGAT2C, 2D exhibited considerably higher activity on eukaryotic DAGs C16:0/C18:1 and C18:1/C18:1 than on the prokaryotic DAGs (Supplemental Figure 5C).

Endogenous Overexpression and Knockdown of NoDGAT2A, 2C, and 2D Reveal Their Distinct *In Vivo* Activities

To probe their *in vivo* activities, we overexpressed *NoDGAT2A*, *2C*, and *2D* and knocked each of them down in *N. oceanica* IMET1 (Supplemental Figures 2 and 3; Supplemental Methods; Methods). For each of the three *NoDGAT2s* under every direction of controlled transcription, two independent, validated lines were characterized in depth (Methods).

Phenotypes of NoDGAT2A-Transgenic Lines

Compared with the control, *NoDGAT2A* transcript exhibited 3.1- to 9.6-fold increase in its overexpression lines (2Ao1 and 2Ao2), and 59.5%–80.4% reduction in its knockdown lines (2Ai1 and 2Ai2) at 0 h, 6 h, 24 h, and 48 h under N-depleted conditions (N−) (Figure 3A). Significant differences ($p \leq 0.05$) in TAG content were observed in both knockdown lines at 96 h and in the overexpression lines at 72 h and 96 h. For the *2A*-knockdown lines, TAG content was reduced by 26.1% and 16.3%, respectively (at 96 h under N−; Figure 3B), which, however, was accompanied by 34.6% and 35.2% higher average growth rate than empty vector (EV) (Supplemental Figure 6A). In contrast, in the 2A-overexpression lines, TAG content increased by 20.3% and 31.0%, and TAG productivity rose by 34.6% and 36.5% (at 96 h under N−; Supplemental Figure 6B), yet growth curves remained unchanged (Supplemental Figure 6A).

Moreover, in the *2A*-overpression lines, at 96 h under N−, the level of TAG-associated SFAs (C14:0, C16:0 and C18:0) increased by 11.6% and 15.0%, while MUFAs (C16:1 and C18:1) decreased by 25.9% and 32.5% (Figure 3C and Supplemental Figure 7A). By contrast, in the *2A*-knockdown lines, TAG-associated SFAs reduced by 7.7% and 7.8%, respectively, while MUFAs rose by 13.4% and 12.5%. However, none of the PUFAs (C18:2, C18:3, C20:4, and C20:5) exhibited significant difference between transgenic lines and EV (except 2Ao1; Figure 3C).

Change of TL-associated FAs (especially C14:0, C16:0, and C16:1) in the *2A*-transgenic lines followed a trend similar to that in TAG-associated FAs at 96 h under N− (Figure 3D). In the two *2A*-overexpression lines, SFAs in TLs increased by 7.1% and 7.8% while MUFAs in TLs decreased by 6.3% and 6.1%. In the *2A*-knockdown lines, SFAs in TLs were reduced by 6.9% and 7.6% while MUFAs in TLs rose by 4.3% and 5.6%. Meanwhile, there was little change of total FAs in the transgenic lines as compared with EV at 0 h, 24 h, 48 h, and 72 h under N− (Supplemental Figure 7B). Therefore, the *in vivo* activity of *2A* is largely consistent with the *in vitro* and *ex vivo* activities, and it can be exploited to specifically boost the relative abundance of SFAs over MUFAs in both TAGs and TLs.

Phenotypes of NoDGAT2C-Transgenic Lines

Compared with EV, *NoDGAT2C* transcript exhibited a 4.7- to 14.9-fold increase in its overexpression lines (2Co1 and 2Co2), and 64.4%–75.7% reduction in knockdown lines (2Ci1 and 2Ci2) (at 0 h, 6 h, 24 h, and 48 h under N−; Figure 4A).

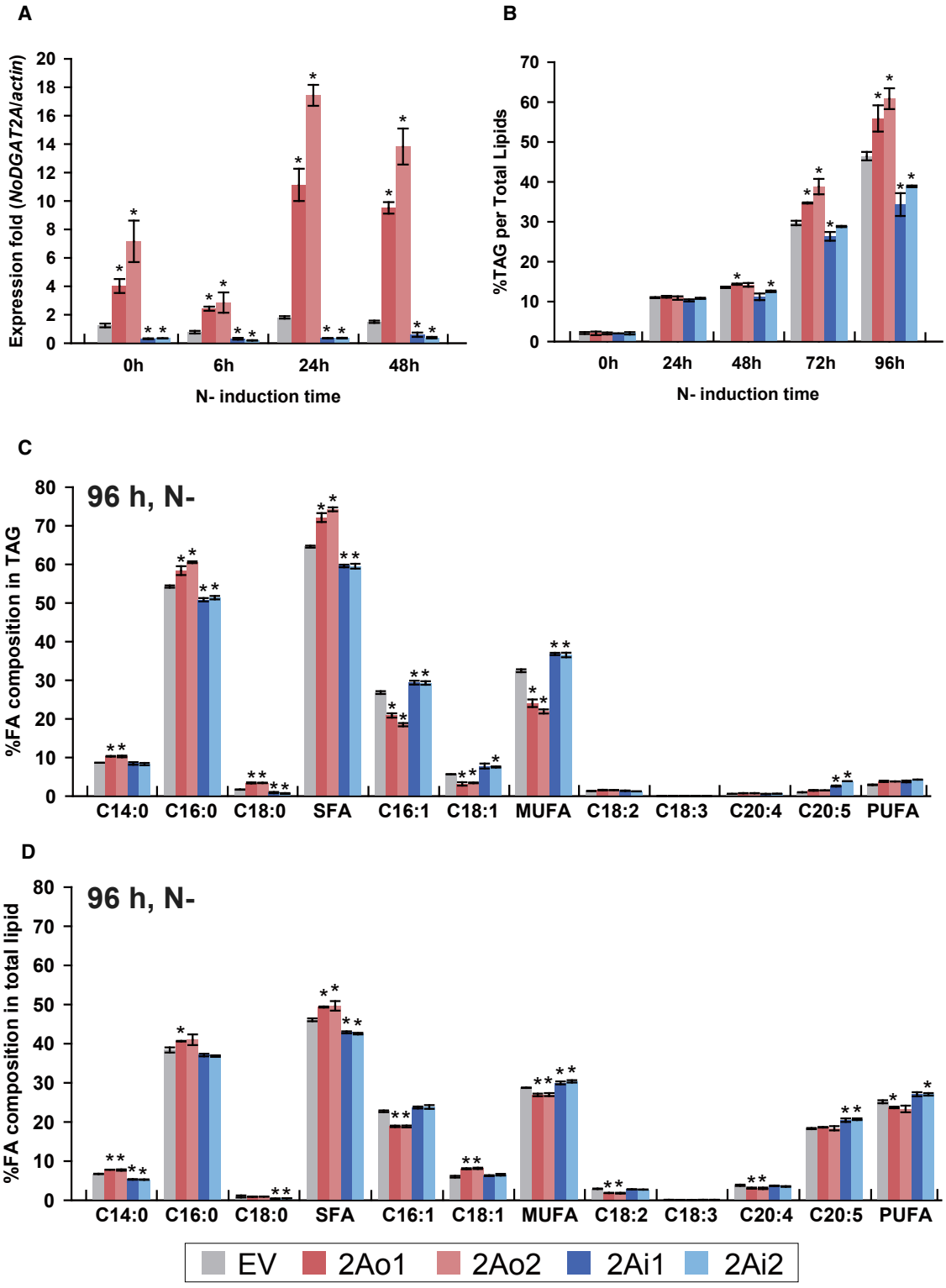

Figure 3. Phenotypes of *NoDGAT2A* Overexpression and Knockdown *N. oceanica* Lines.

(A) Transcript levels of *NoDGAT2A* in the two *2A* overexpression lines (2Ao1 and 2Ao2) and the two *2A* knockdown lines (2Ai1 and 2Ai2) plus an empty vector control (EV) under N+ (0 h) and N− (6 h, 24 h, and 48 h after induction), as measured by qRT–PCR. Transcription level of *NoDGAT2A* was normalized to that of β-actin, the internal control.

(B) TAG content the *NoDGAT2A* overexpression and knockdown lines under N+ (0 h) and N− (24 h, 48 h, 72 h, and 96 h after induction).

(C) FA composition of TAG in the *NoDGAT2A* overexpression and knockdown lines under N− (96 h after induction).

(D) FA composition of total lipids in the *NoDGAT2A* overexpression and knockdown lines under N− (96 h after induction).

Data represent mean ± SD ($n = 3$). An asterisk indicates significance by Student's *t*-test ($p \leq 0.05$).

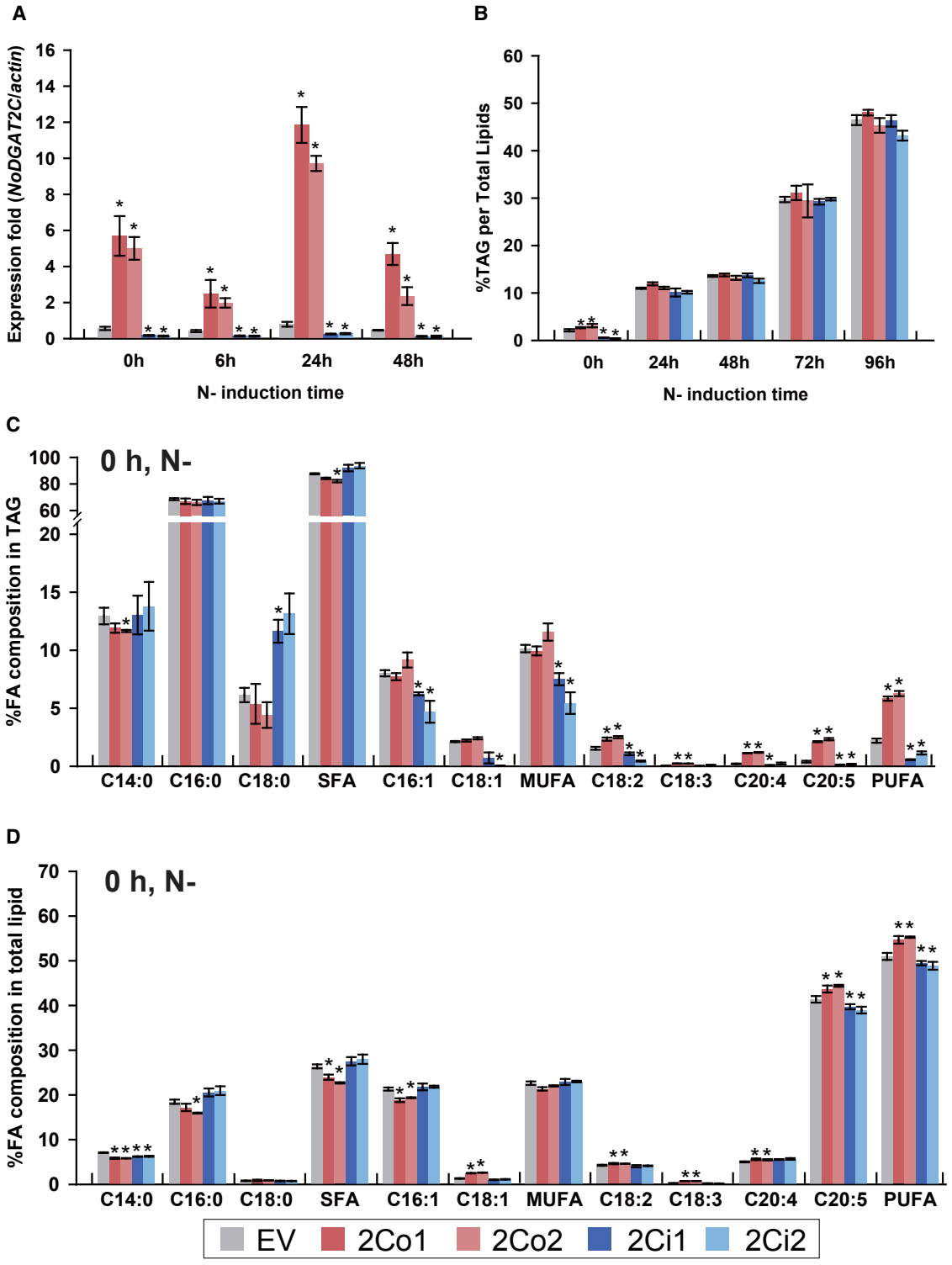

Figure 4. Phenotypes of *NoDGAT2C* Overexpression and Knockdown *N. oceanica* Lines.

(A) Transcript levels of *NoDGAT2C* in the two *2C* overexpression lines (2Co1 and 2Co2) and the two *2C* knockdown lines (2Ci1 and 2Ci2) plus an empty vector control (EV) under N+ (0 h) and N− (6 h, 24 h, and 48 h after induction), as measured by qRT–PCR. Transcription level of *NoDGAT2C* was normalized to that of β-actin, the internal control.

(B) TAG content of the *NoDGAT2C* overexpression and knockdown lines under N+ (0 h) and N− (24 h, 48 h, 72 h, and 96 h after induction).

(C) FA composition of TAG in the *NoDGAT2C* overexpression and knockdown lines under N+.

(D) FA composition of total lipids in the *NoDGAT2C* overexpression and knockdown lines under N+.

Data represent mean ± SD ($n = 3$). An asterisk indicates significance by Student's *t*-test ($p \leq 0.05$).

Significant differences ($p \leq 0.05$) in TAG content were only observed at 0 h in the *2C*-knockdown and -overexpression lines. The *2C*-overexpression lines grew 7.7% and 9.6% slower than EV, yet the *2C*-knockdown lines grew 30.8% and 23.1% faster (Supplemental Figure 6C). Overexpression of *2C* resulted in an increase in TAG content by 26.0% and 45.9%, respectively in the 2Co1 and 2Co2 lines, and an increase in TAG productivity by 70.2% and 100.5%, respectively in the 2Ci1 and 2Ci2 lines (at 0 h; Figure 4B). In contrast, *2C* knockdown led to a reduction of TAG content by 72.3% and 81.0% and a reduction of TAG productivity by 54.8% and 70.9%, respectively, in the 2Ci1 and 2Ci2 lines (at 0 h under N−; Supplemental Figure 6D).

Among the TAG-associated FAs, profiles of SFAs and MUFAs in the *2C* transgenic lines were largely similar to EV, but this was not the case for PUFAs. Compared with EV, the level of PUFAs in TAG increased by 164.2% and 184.0% (C18:2 by 51.1% and 62.3%; C18:3 by 367.3% and 351.8%; C20:4 by 442.4% and 470.2%; C20:5 by 430.1 and 484.4%) in the *2C*-overexpression lines, while it reduced by 74.4% and 48.1% (C18:2 by 30.7% and 70.9%; C18:3 by 31.1% and 8.2%; C20:4 by 56.5% and 10.8%; C20:5 by 70.0% and 56.7%) in the *2C*-knockdown lines (all at 0 h under N−; Figure 4C and Supplemental Figure 8A).

Change of TL-associated PUFAs between the *2C*- transgenic lines and EV was largely similar to that of PUFAs in TAGs (Figure 4D). PUFAs in TLs increased by 7.3% and 8.5% (EPA in TLs increased by 5.6% and 7.3%) in the two *2C*-overexpression lines, and were reduced by 2.9% and 4.1% (EPA in TLs reduced by 4.0% and 5.8%) in the *2C*-knockdown lines. Meanwhile, total FAs in the transgenic lines were unchanged as compared with EV at 24 h, 48 h, 72 h, and 96 h under N− (Supplemental Figure 8B). Therefore, *NoDGAT2C* appeared to specifically target PUFAs *in vivo*, which can be employed to modulate the proportion of PUFAs in both TAGs and TLs.

Phenotypes of NoDGAT2D-Transgenic Lines

Compared with EV, *NoDGAT2D* transcript exhibited a 4.3- to 8.0-fold increase in its overexpression lines (2Do1 and 2Do2) and 73.6%–79.8% reduction in its knockdown lines (2Di1 and 2Di2) (at 0 h, 6 h, 24 h, and 48 h under N−; Figure 5A). Significant differences ($p \leq 0.05$) in TAG content were observed in both knockdown lines at 0 h, 24 h, and 96 h and overexpression lines at 24 h. For *2D*-overexpression lines no growth slowdown was apparent, yet TAG content increased by 23.4% and 28.3% (at 24 h under N−) and TAG productivity rose by 24.2% and 32.8% (at 24 h under N−; Figure 5B). By contrast, for the *2D*-knockdown lines, average growth rate was 44.2% and 38.5% higher than in EV (Supplemental Figure 6E); TAG content was reduced by 80.2% and 81.7% at 0 h and by 78.3% and 74.8% at 24 h under N− (by 47.4% and 45.1% at 96 h under N−; Figure 5B), while TAG productivity decreased by 68.5% and 71.4% at 0 h and by 87.4% and 85.0% at 24 h under N− (Supplemental Figure 6F).

Among the TAG-associated FAs, levels of SFAs and PUFAs in the *2D*-transgenic lines were largely similar to EV (e.g., at 24 h under N−). However, the level of MUFAs increased by 23.0% and 30.8% (C16:1 by 15.0% and 23.7%; and C18:1 by 223.1% and 206.7%) in the *2D*-overexpression lines, yet decreased by 52.0% and 64.5% (C16:1 by 51.5% and 64.9%; and C18:1 by 64.6% and 55.1%) in the *2D*-knockdown lines (at 24 h under N−; Figure 5C and Supplemental Figure 9A).

Change of TL-associated FAs in *2D*-transgenic lines followed a trend similar to their counterparts in TAGs (at 24 h under N−; Figure 5D and Supplemental Figure 9B). In the *2D*-overexpression lines, the level of MUFAs in TLs increased by 12.6% and 15.6% while that of SFAs decreased by 4.7% and 3.9%. By contrast, in the *2D*-knockdown lines MUFAs in TLs decreased by 38.5% and 36.2% whereas SFAs increased by 20.0% and 27.2%. Therefore, largely consistent with its *in vitro* and *ex vivo* activities, *NoDGAT2D* prefers MUFAs *in vivo* and this specificity can be exploited to boost the intracellular ratio of MUFAs over SFAs (i.e., the exact opposite effect of *2A*) in both TAGs and TLs.

A Mechanistic Model of TAG Assembly in *N. oceanica*

Evidence from reverse genetics analysis above thus revealed a *NoDGAT2* teamwork featuring distinct yet complementary activities among *NoDGAT2A*, *2C*, and *2D* in substrate preference and product selectivity *in vivo* (Supplemental Table 3). The consequence is profound: in wild-type *N. oceanica*, under both N+ (Supplemental Figure 10A) and N− (Supplemental Figure 10B), at each of the six time points sampled the content of TAG-derived SFAs was 2.29- to 5.70-fold that of TAG-derived MUFAs, which in turn was 1.03- to 5.45-fold that of TAG-derived PUFAs. In fact, this rigid hierarchy was strictly obeyed by *NoDGAT2A*, *2D*, and *2C* in order, whose transcript abundance linearly corresponded to TAG-derived SFAs, MUFAs, and PUFAs, respectively across all samples (r^2 of 0.84 ± 0.13 under N+ and 0.82 ± 0.11 under N−; Supplemental Figure 10). Furthermore, during N− induced TAG biosynthesis, between-condition fold change (i.e., N−/N+) of *NoDGAT2A*, *2C*, and *2D* transcripts exhibited temporal synergy with that of TAG-derived SFAs, MUFAs, and PUFAs, respectively (Supplemental Figure 11A–11C and Supplemental Methods). Thus the TAG-associated SFA/MUFA/PUFA ratio appears to be precisely and rigidly determined by the relative abundance of *NoDGAT2A*, *2D*, and *2C* transcripts under both N+ and N− (Supplemental Figure 10).

Taken together, the polyphyletic origin, stratified yet complementary substrate preference, distinct product profile, hierarchical transcript abundance, and precisely regulated temporal expression pattern of the three *NoDGATs*, plus their specialized subcellular spatial localization (with 2A at endoplasmic reticulum [ER]; such localization of its ortholog in *N. oceanica* CCMP1779 was recently validated via fluorescent labeling of the protein [Zienkiewicz et al., 2017], 2C at plastid, and 2D at the other organelles [prediction using SignalP, ChloroP, Mitoprot, and HECTAR based on their signaling sequences; Li et al., 2014; Wang et al., 2014]), unveiled an *in vivo* mechanism of TAG synthesis in *N. oceanica*. Here three TAG assembly routes, each mediated mainly by one of the three NoDGAT2s, collaboratively form the TAG sink from acyl-CoAs and DAGs (Figure 6). (i) The "NoDGAT2A route," which prefers SFAs and primarily produces SFA-TAGs via the ER-targeted, green-algae-originated *NoDGAT2A*, presumably

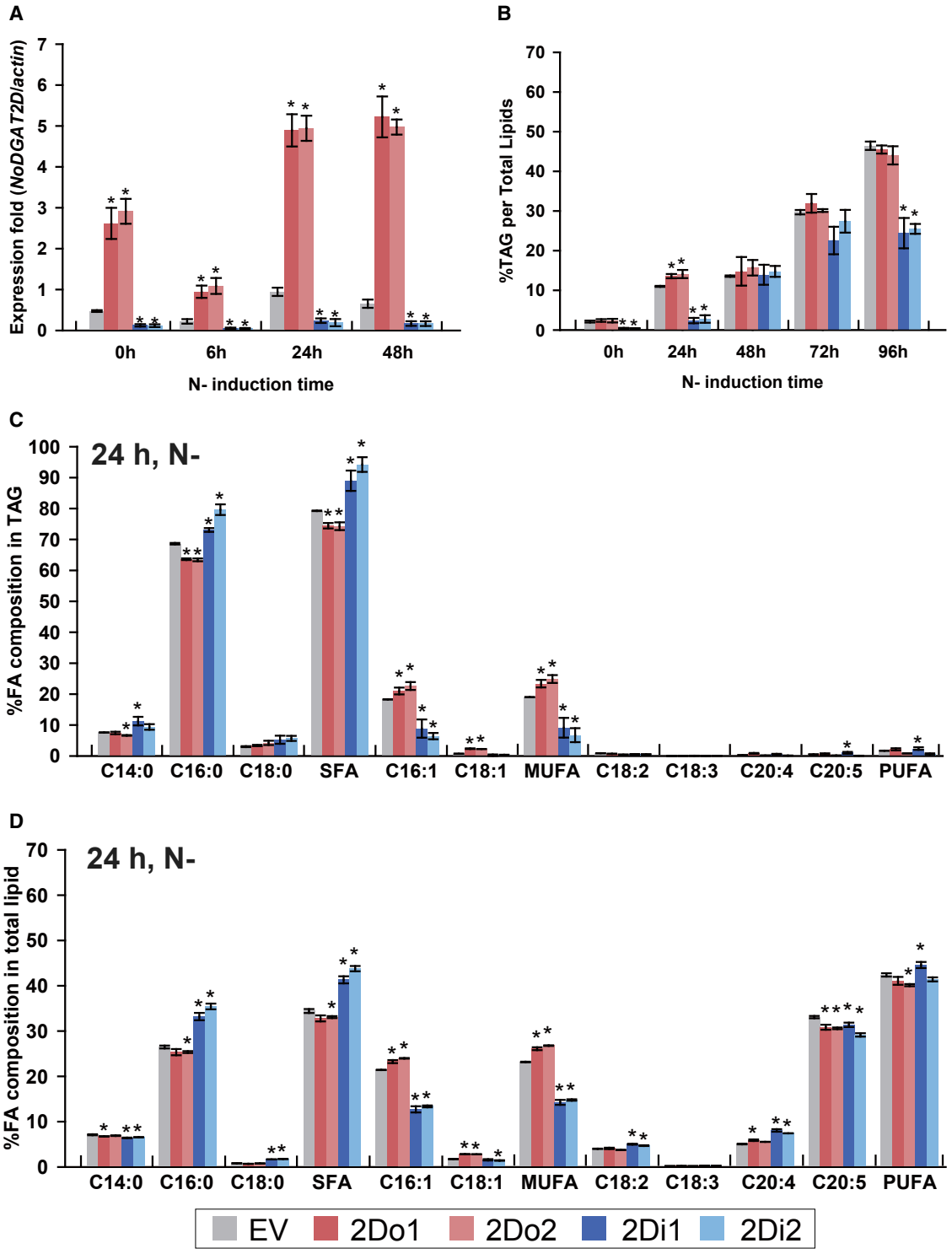

Figure 5. Phenotypes of *NoDGAT2D* Overexpression and Knockdown *N. oceanica* Lines.

(A) Transcript levels of *NoDGAT2D* in the two *2D* overexpression lines (2Do1 and 2Do2) and the two *2D* knockdown lines (2Di1 and 2Di2) plus an empty vector control (EV) under N+ (0 h) and N− (6 h, 24 h, and 48 h after induction), as measured by qRT–PCR. Transcription level of *NoDGAT2D* was normalized to that of β-actin, the internal control.

(B) TAG content of the *NoDGAT2D* overexpression and knockdown lines under N+ (0 h) and N− (24 h, 48 h, 72 h, and 96 h after induction).

(C) FA composition of TAG in the *NoDGAT2D* overexpression and knockdown lines under N− (24 h after induction).

(D) FA composition of total lipids in the *NoDGAT2D* overexpression and knockdown lines under N− (24 h after induction).

Data represent mean ± SD ($n = 3$). An asterisk indicates significance by Student's *t*-test ($p \leq 0.05$).

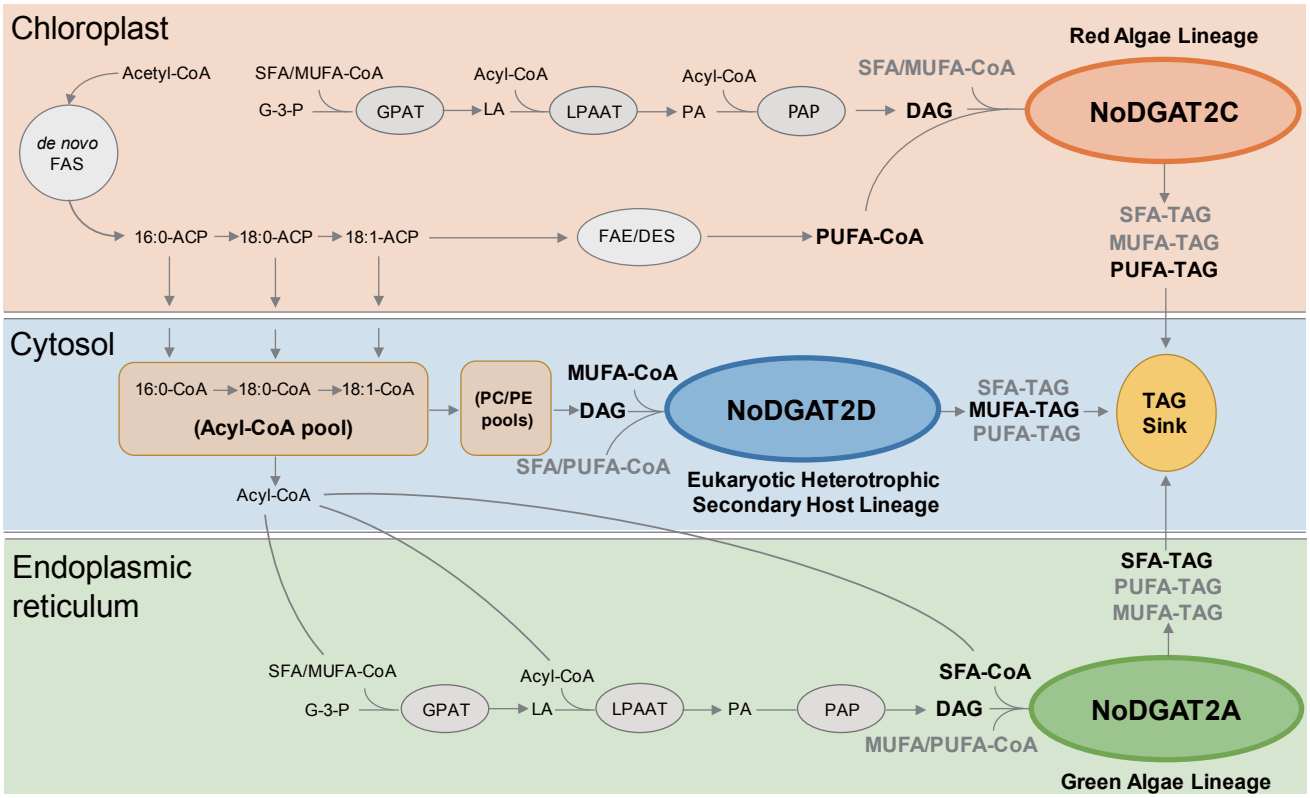

Figure 6. Mechanistic Model of the TAG Assembly Lines Mediated by the Three Polyphyletic *NoDGAT2*s.
For simplicity, a single TAG sink is shown. Not all intermediates or reactions are displayed. In *N. oceanica* CCMP1779, the ortholog of NoDGAT2A has been shown to target ER via fluorescent labeling (Zienkiewicz et al., 2017), while localization of 2C and 2D was *in silico* predicted via SignalP, ChloroP, Mitoprot, and HECTAR in our past studies (Li et al., 2014; Wang et al., 2014), and experimental evidence has not yet been available. Black boldface fonts of FA-CoAs and FA-TAGs represent the primary substrates and the major products of a particular NoDGAT2. Arrows indicate catalytic steps in the pathway. ACP, acyl carrier protein; DAG, diacylglycerol; DES, desaturase; FA, fatty acid; FAE, fatty acid elongase; FAS, fatty acid synthase; G-3-P, glycerol-3-phosphate; GPAT, glycerol-3-phosphate acyltransferase; LA, lysophosphatidic acid; LPAAT, lysophosphatidic acid acyltransferase; MUFA, monounsaturated fatty acids; PA, phosphatidic acid; PAP, phosphatidic acid phosphatase; PC, phosphatidylcholine; PE, phosphatidylethanolamine; PUFA, polyunsaturated fatty acid; SFA, saturated fatty acid; TAG, triacylglycerol.

takes place in ER, consistently exhibits the highest transcript level among the three *NoDGAT2*s, is upregulated in transcript abundance starting at ~6 h after N−, and contributes the bulk of total TAG biosynthesized. (ii) The "NoDGAT2C route," which exhibits a stronger preference for PUFAs than the other two routes and produces PUFA-TAGs via the plastid-targeted, red-algae-originated *NoDGAT2C*, likely operates at the chloroplast outer envelope or chloroplast-ER (cER), as indicated by evidence from related DGATs in *C. reinhardtii* (Liu et al., 2016b) or *N. oceanica* (Wei et al., 2017a), consistently exhibits the lowest transcript level among the three *NoDGAT2s*, is upregulated in transcript level starting at ~12 h after N− onset, and serves as a relatively small contributor to total TAG biosynthesized. (iii) The "NoDGAT2D route," which prefers MUFAs and primarily produces MUFA-TAGs via the eukaryotic-heterotrophic-secondary-host derived *NoDGAT2D*, takes place in the other organelles, consistently exhibits the second highest transcript level among the three *NoDGATs*, is upregulated in transcript level starting at ~6 h after onset of N−, and contributes moderately to total TAG. In the end, these SFA/PUFA/MUFA-TAGs were pooled into various forms of "TAG sink" (e.g., lipid droplets), resulting in the rich content and diverse profile of TAGs in *N. oceanica* (410 mg/g·dry weight [DW] over 96 h under N−; 16 major TAG species [Li et al., 2014]).

Creating *N. oceanica* Strain Bank with a Wide Spectrum of FA-DU in Oils by Rational Modulation of *NoDGAT2A*, *2C*, and *2D*

To test whether the extraordinary features of *NoDGAT2* network can be exploited for designing the SFA/MUFA/PUFA ratio and thus FA-DU of microalgal oils (Table 1), we compared the two overexpression and two knockdown *N. oceanica* lines targeting each of *NoDGAT2A*, *2C*, and *2D* for productivity and profile of TLs, TAGs and their associated SFAs/MUFAs/PUFAs, over the full N− induced TAG biosynthesis processes (i.e., at 0 h, 24 h, 48 h, 72 h, and 96 h under N−).

(i) For TAG productivity, the NoDGAT2s exerted distinct effects, in both direction and extent (Supplemental Figure 12A). Specifically, the top TAG productivity was found at 2Ci1 (172.0 mg/g DW), which is 227.4% of that at the bottom performing line 2Di1 (both at 96 h under N−). Moreover, 2Ao1 and 2Ao2 increased TAG productivity by 16.9% and 12.5%, respectively, compared with EV at 96 h under N−. Thus 2A overexpression or 2C

		Growth rate[a]	TAG[b]					TL[c]					Suitable product derived from TAG or TL
			Content	Productivity	FA-DU value	N value	F value	Content	Productivity	FA-DU value	N value	F value	
NoDGAT2A	Overexpression	–	31.0%↑	36.5%↑	20.8%↓	102.5%↑	52.7%↓	–	–	–	–	–	Nutrient (TAG)
	Knockdown	35.2%↑	26.1%↓	19.0%↓	37.0%↑	–	–	15.9%↓	–	10.5%↓	12.2%↑	20.2%↑	
NoDGAT2C	Overexpression	–	–	14.3%↓	43.5%↑	35.3%↑	13.9%↓	42.2%↑	37.3%↑	17.8%↑	21.5%↑	12.2%↓	Nutrient (TL)
	Knockdown	30.8%↑	–	18.5%↑	31.5%↓	42.3%↓	42.9%↓	26.2%↑	62.9%↑	–	19.5%↓	–	
NoDGAT2D	Overexpression	–	–	32.8%↑	–	72.8%↓	36.1%↑	–	–	–	–	20.1%↑	Fuel (TAG)
	Knockdown	44.2%↑	47.4%↓	43.2%↓	12.0%↓	63.4%↓	56.3%↓	53.2%↓	41.9%↓	18.5%↓	22.9%↓	36.7%↓	

Table 1. Correlation among the Multiple Key Traits of Biotechnological Interest in the *N. oceanica* Mutant Bank.

Note: values indicate the percentage fold change as compared with EV. ↑, upregulation; ↓, downregulation; –, ≤10%.

[a]Average growth rate under N+.

[b]96 h under N−.

[c]0 h under N−.

inhibition can both elevate TAG productivity. Modulation of NoDGAT2s also generated a wide spectrum of profile in TAG-associated FAs (Supplemental Figure 12A): at 96 h, the highest and lowest proportions of SFAs were found at 2Di2 (77.1%) and 2Ai2 (59.5%), respectively; for MUFAs the former was at 2Do1 (37.5%) while the latter at 2Di2 (20.8%); for PUFAs the former was at 2Ai2 (4.3%) yet the latter was at 2Do1 (1.3%).

(ii) For TL productivity (Supplemental Figure 12B), the best performance was found at 2Ci1 (344.7 mg/g DW), which is 148.1% of the lowest at 2Co1 (both at 96 h under N−). Interestingly, relative to EV, TL productivity was elevated (by 1.1%–23.1%) in nearly all knockdown lines (except 2Ai2), while reduced (by 1.6%–16.8%; all at 96 h under N−) in all overexpression lines. This is consistent with the role of NoDGAT2A, 2C, and 2D in pulling the intracellular pool of carbon into synthesis of TAG and demonstrates a strategy for enhancing TL productivity. Similarly, tuning of NoDGAT2s can also modulate the FA profile in TLs: for SFAs, at 96 h, the highest and lowest proportions were at 2Di2 (54.6%) and 2Ai2 (42.6%), respectively; for MUFAs they were at 2Ai2 (31.0%) and 2Di2 (23.0%); for PUFAs they were at 2Co1 (27.6%) and 2Di2 (22.3%) (Supplemental Figure 12B). Notably, for a given transgenic line, changes of FA profile in TLs were largely consistent with (yet milder than) that in TAGs. Thus, tuning of NoDGAT2s can modulate both productivity and FA profile of TLs, in addition to those of TAGs.

(iii) As for the productivity of PUFAs (LA, ALA, ARA, and EPA, all essential FAs of human; Supplemental Figure 12C), which was generally higher in the early phase of nitrogen depletion (0 h and 24 h under N−) than in the later phases (48 h, 72 h, and 96 h under N−), the peak performance was found in 2Ci1 (116.1 mg/g DW), which is 175.1% of the poorest line 2Do2 (both at 0 h under N−). Surprisingly, all transgenic lines except 2Do1 and 2Do2 featured higher PUFA productivity (by up to 51.0%) than EV, revealing multiple routes in genetically engineering this trait. As for the profile of PUFAs, a NoDGAT2 gene-specific effect was apparent and a wide diversity of PUFA profile was found among the strain bank (Supplemental Figure 12C). Specifically, at 0 h the highest proportion of C18:2 (LA) was found at 2Di1 (12.1%) with the lowest at 2Ci1 (8.2%); for C18:3 (ALA) they were at 2Co1 (1.4%) and 2Ci2 (0.4%); for C20:4 (ARA) they were at 2Di2 (15.8%) and 2Ao2 (9.7%); for C20:5 (EPA) they were at 2Ao2 (81.4%) and 2Di1 (71.7%).

As PUFAs and MUFAs are respectively the primary determinant of suitability of microalgal oils as nutrient supplements and fuels (Ramos et al., 2009; Horn and Benning, 2016), "N value" (defined as $10^{(\%\text{PUFA in transgenic line})/(\%\text{PUFA in EV})}$) and "F value" (i.e., $10^{(\%\text{MUFA in transgenic line})/(\%\text{MUFA in EV})}$) were proposed respectively and calculated for each line in the strain bank (Figure 7A and 7B) to quantitatively compare each line's potential (relative to the wild-type) to serve as feedstock for nutrient supplements versus that for fuels. Moreover, "FA-DU value" of TAG (or TL) was defined as $10^{(\text{FA−DU in transgenic line})/(\text{FA−DU in EV})}$, so as to quantify the extent to which a line is engineered toward higher or lower FA-DU. The *NoDGAT2A/2C/2D* overexpression or knockdown lines represented a wide spectrum of TAG-derived applications, from those particularly suitable for nutrient supplements (e.g., 2Ao1

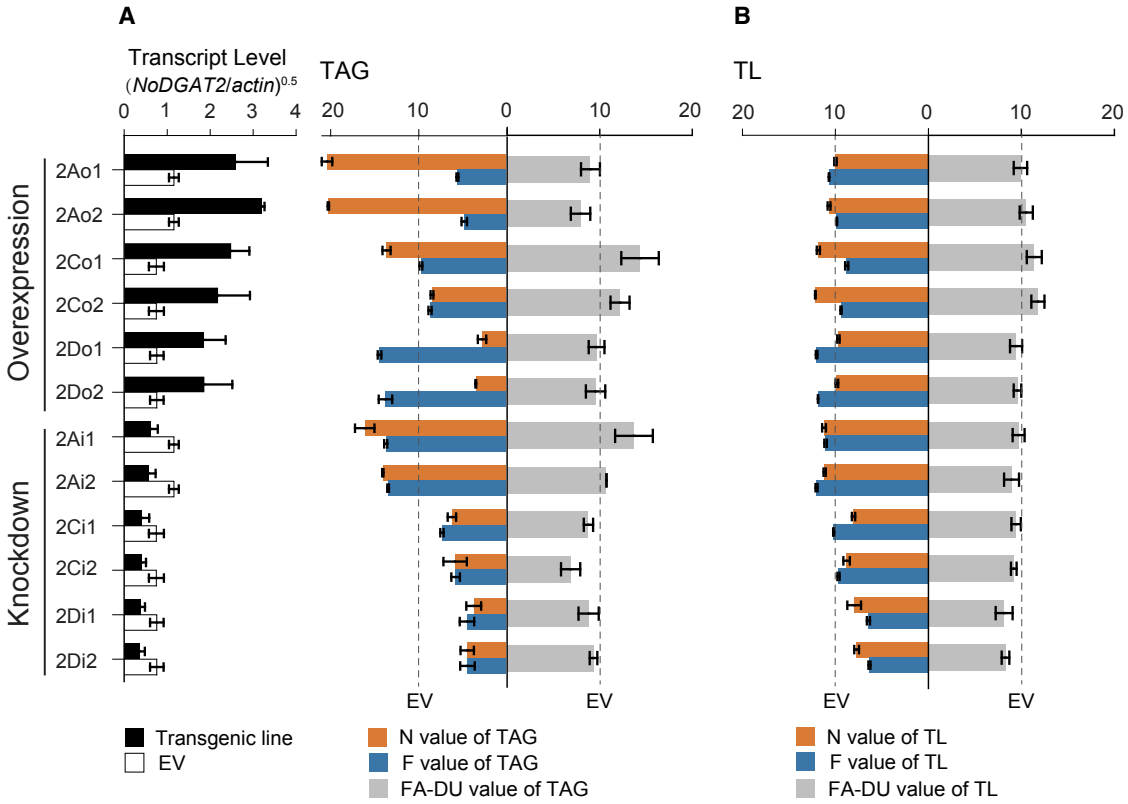

Figure 7. Rational Regulation of FA Composition in *NoDGAT2* Overexpression and Knockdown Lines of *N. oceanica*.

N value, F value, and FA-DU value of TAG at 96 h under N− **(A)** and those of TL at 0 h under N− **(B)** are shown. The transcript levels ($(NoDGAT2/actin)^{0.5}$) of transgenic line and EV are shown by bars (black: transgenic line; white: EV). "FA-DU value" ($10^{(\text{FA-DU in transgenic line})/(\text{FA-DU in EV})}$; (FA-DU) = (%C16:1 + %C18:1) × 1 + (%C18:2) × 2 + (%C18:3) × 3 + (%C20:4) × 4 + (%C20:5) × 5) was calculated to evaluate the preference as nutrient supplements over biofuels. Data represent mean ± SD (n = 3). N value of a given line is defined as $10^{(\%\text{PUFA in transgenic line})/(\%\text{PUFA in EV})}$, while F value is defined as $10^{(\%\text{MUFA in transgenic line})/(\%\text{MUFA in EV})}$. N value of >10 and F value of >10 indicates that the line is more suitable for production of nutritional supplement and for fuel, respectively.

and 2Ao2) to those tailored for fuels (e.g., 2Do1 and 2Do2; Figure 7A). Further analysis revealed the following.

(i) As TAG productivity peaked at 96 h under N− (Supplemental Figure 12A), N value and F value of TAGs were evaluated at this time point (Figure 7A). 2Ao1, 2Ao2, and 2Co1 exhibited 102.5%, 101.1%, and 35.3% higher N value than EV, while 2Do1 and 2Do2 exhibited 72.8% and 65.7% higher F value than EV. As for FA-DU value, those of 2Co1 and 2Co2 reached 14.4 and 12.2 while those of 2Ao1 and 2Ao2 were as low as 9.0 and 7.9 (the FA-DU value of EV is 10). Thus N and F values and FA-DU value of TAGs can be greatly elevated by overexpressing specific NoDGAT2s, with 2A- and 2C-overexpression lines more suitable for production of nutritional supplements and 2D-overexpression lines suitable for fuels.

(ii) Considering that productivity of total PUFAs peaked at 0 h under N− (Supplemental Figure 12C), N value and F value of TLs were assessed at this time point (Figure 7B). Compared with EV, 2Co1, 2Co2, 2Ai1, and 2Ai2 exhibit 18.2%, 21.5%, 12.2%, and 11.6% higher level in N value, while 2Do1, 2Do2, 2Ai1, and 2Ai2 increased by 20.1%, 18.7%, 10.5%, and 20.2% in F value. As for FA-DU value, those of 2Ao2, 2Co1, and 2Co2 reached 10.5, 11.4, and 11.8 while those of 2Di1 and 2Di2 were as low as 8.2 and 8.3. Therefore, N value, F value and FA-DU value of *N. oceanica* TLs can be tuned (though to a lesser degree than TAGs), especially via modulating 2C and 2D, whereby 2C-overexpression lines are more suitable for nutritional supplement production while 2D-overexpression lines are suitable for biofuels. Thus the present line panel spanned a dynamic range of FA-DU value (7.9–14.4 in TAG and 8.2–11.8 in TL), underscoring the excellent flexibility of this strategy for producing "designer oils."

Notably, interactions among the multiple traits related to growth rate, oil productivity, and oil property were apparent (Table 1). (i) Transcript abundance of *NoDGAT2A/C/D* is positively correlated with TAG productivity yet negatively correlated with growth rate of the microalga (knockdown of all three genes leads to faster grow rate). (ii) It is feasible to simultaneously enhance growth rate, TAG productivity, and N value, as exemplified by the *NoDGAT2A* overexpression lines. (iii) Simultaneous improvement of growth rate, TAG productivity, and F value is also possible, as demonstrated by *NoDGAT2D* overexpression. (iv) TL productivity and N value can be improved together, by *NoDGAT2C* overexpression. (v) Both N value and F value of TLs can be improved without compromising the productivity of TLs, as shown in the *NoDGAT2A* knockdown lines. Therefore, an optimal

combination of key industrial traits can be integrated into a single strain by carefully tuning the absolute and relative abundance of the *NoDGAT2s*.

DISCUSSION

Secondary endosymbiosis greatly contributed to the genetic diversity on Earth and gave birth to many of the microalgal lineages that are still present today (Archibald, 2009). In this ancient event, a heterotrophic eukaryotic cell engulfed at least one photosynthetic microalgal cell that had undergone primary endosymbiosis (a green or red algal cell, or both of them). Endosymbiotic gene transfer has been proposed as one major driving force for the interplays among the participating genomes, but how such interplay resulted in or shaped the function and evolution of algal genomes remained elusive (Timmis et al., 2004; Zimorski et al., 2014).

Our *in silico*, *ex vivo*, *in vitro*, and *in vivo* results here showed that the large number of *DGAT*s in the model oleaginous microalga *N. oceanica*, despite the generally much smaller genome sizes (Radakovits et al., 2012; Vieler et al., 2012; Wang et al., 2014), can be explained by the symbiosis of *NoDGAT*s that originated from the three participating ancestral genomes of secondary endosymbiosis, whereby indigenous and adopted *DGAT*s have co-evolved in the new host cell and eventually formulated a multi-dimensional partnership that features the complementary talents, functional specialization, and synergetic teamwork among the NoDGATs. This is quite distinct from higher plants and green algae, where genome duplication followed by duplication or loss of specific genes has been frequently recruited to explain the evolution of paralogous gene families (Lan et al., 2009; Shoji and Hashimoto, 2011). Although whether the substrate preferences of NoDGAT2A, 2C, and 2D are inherited from respective ancestors or subsequently acquired during the co-evolution in the new host cells is not clear, it appears that the consequence of *NoDGAT2* co-evolution is a spatially, temporally, evolutionarily, and functionally heterogeneous yet coordinated cell factory of TAG, with synergy and complementarity in transcript abundance, temporal gene expression pattern, subcellular spatial localization, substrate preference, and product profile among the NoDGAT2s. This has important implications in environmental adaptation in microalgae. For example, the distinct subcellular localization of NoDGAT2s may partition TAG assembly into various compartments of microalgal cells. Moreover, the sequential and coordinated upregulation responses of the three *NoDGAT2* transcripts under N− suggested an assembly-line-like manner for TAG synthesis for rapidly and efficiently responding to environmental stresses, under certain regulatory mechanisms such as transcription factor (Boyle et al., 2012; Hu et al., 2014) and/or alternative splicing (Guiheneuf et al., 2011). Finally, it is also possible that the preference for acyl-CoAs of different degrees of saturation among NoDGAT2A, 2C, and 2D represents a mechanism to maintain the homeostasis between saturated and unsaturated FA in microalgae, which is critical for the stabilization of intracellular membrane systems.

Underlying this evolutionary feat is the convergence of at least five juxtaposing forces on *NoDGAT2A*, *2C*, and *2D*: (i) high degree of genetic divergence due to the distinct ancestors; (ii) functional divergence featuring distinct yet complementary substrate preference and TAG product profile; (iii) rather rigid hierarchy in transcript abundance with *2A* staying on top and *2C* at the bottom, which directly determines the relative abundance of SFAs/MUFAs/PUFAs; (iv) temporal labor division of TAG synthesis, as evidenced by the differential gene regulation that creates distinct temporal patterns of transcript abundance; and (v) highly heterogeneous yet coordinated spatial organization of NoDGATs across multiple subcellular localizations. Recognition of each of the forces creates opportunities to develop ''designer microalgae'' for producing oils with the proper FA profile, FA-DU, and other industrial traits. Here, by series overexpression or knockdown of *NoDGAT2A*, *2C*, and *2D*, we established a bank of *N. oceanica* strains optimized for either nutrient or fuel production and together spanning a wide range of FA-DU, where proportions of SFAs, MUFAs, and PUFAs in TAG varied by 1.3-, 3.7-, and 11.2-fold. Thus designer FA profiles with targeted FA-DU and with designated SFA/MUFA/PUFA ratios in both TAGs and TLs can be created based on the FA substrate preference and relative transcript level of 2A/2C/2D in *N. oceanica*. In particular, preference of NoDGAT2C to PUFAs can be exploited for overproducing PUFA (particularly EPA and its precursors), thus increasing the nutritional value of microalgal oils—its overexpression resulted in up to 184.0% increase in TAG-associated PUFA (Figure 4C and 4D); while NoDGAT2D's preference for MUFAs can be exploited for producing better fuels, as its overexpression led to up to 30.8% and 15.6% increase in TAG- and TL-associated MUFA, respectively (Figure 5C and 5D).

Moreover, in addition to the SFA/MUFA/PUFA ratio, growth rate and TAG productivity can be rationally engineered by fine-tuning the absolute abundance of *NoDGAT2A*, *2C*, and *2D*. For example, *2A* overexpression led to simultaneous improvement of TAG productivity and high-value nutrient (PUFAs) production, while lines overexpressing *2C* featured enhanced TL productivity plus multi-fold overproduction of key PUFAs (e.g., LA by 51.1% and 62.3%; ALA by 367.3% and 351.8%; ARA by 442.4% and 470.2%; EPA by 430.1 and 484.4%). Notably, in *N. oceanica* CCMP1779, overexpression of *NoDGTT5* (ortholog of *NoDGAT2A* in *N. oceanica* IMET1; Supplemental Table 1), which exhibited TAG-synthetic activity both *in vitro* and in yeast, led to higher TAG content, lower growth rate, and slight change in relative abundance of C16 and C18 (Zienkiewicz et al., 2017). On the other hand, *2C* knockout led to improved growth rate, plus elevated productivity of both TAG and TL. As NoDGAT2C is predicted to be located at the chloroplast outer envelope or cER, these results are in line with our previous hypothesis that inhibition of prokaryotic TAG biosynthesis may increase TAG productivity (Liu et al., 2016b).

In higher plants, the main strategy to engineer FA-DU is via desaturases and elongases (Chiron et al., 2015; Lee et al., 2016). In microalgae, although a number of desaturases (Tonon et al., 2005; Iskandarov et al., 2010) or elongases (Yu et al., 2012; Dolch et al., 2017) were characterized, success stories of FA-DU engineering are rare. One notable example is in *N. oceanica* CCMP1779, where overexpression of four FA desaturases led to considerable increases in the proportion of long-chain PUFAs including EPA in TL (but not in TAG [Poliner et al., 2017]). Compared with those focusing on desaturases/elongases, DGAT2-targeted strategies can offer significant advantages, due to: (i) their specific modulation of FA-DU for TAG (which is

the main ingredient of neutral lipids accumulated under industrial production) rather than for TL; (ii) their ability to introduce a high degree of alteration to FA profile in TAG, i.e., proportion of SFAs, MUFAs and PUFAs in TAG varied by 1.3-, 3.7-, and 11.2-fold (4.8-fold increase for EPA); (iii) their flexibility and potentially wider dynamic range of rational tuning, by exploiting the extraordinary multiplicity of *DGAT2* genes co-inhabiting in a single microalgal cell; (iv) their ability to simultaneously improve not only oil properties but also oil productivity.

Finally, our understanding and exploitation of the DGAT functional network in *N. oceanica* or for oleaginous microalgae in general have only just begun. Although only NoDGAT2A, 2C, and 2D exhibit *ex vivo* TAG-synthetic activity in yeast, the other NoDGATs (or some of them [e.g., Li et al., 2016; Wei et al., 2017a]) might be active for TAG synthesis *in vivo*, as the difference in substrate profile and subcellular structure between yeast and *Nannochloropsis* spp. may explain the discrepancy of activity profile between the two hosts. As the next step, simultaneous and combinatorial modulation of the complete set of *NoDGATs* via the rapidly expanding *Nannochloropsis* genetic toolbox, e.g., genome editing (Wang et al., 2016; Ajjawi et al., 2017), gene knockdown (Wei et al., 2017b), and homologous recombination (Dolch et al., 2017; Gee and Niyogi, 2017), should unveil the global metabolic and regulatory network of DGAT2 at a finer resolution and fulfill the potential of "designer industrial microalgae" for robust yet flexible production of fuels and nutritional products. On the other hand, our experimental design here did not attempt to simulate the periodic high/low light and temperature changes and the gradual depletion of nitrogen and other conditions that are typically encountered in a large-scale, outdoor cultivation. Thus the phenotypes of the transgenic *N. oceanica* lines need be further validated under biotechnologically relevant growth conditions. Nevertheless, the recognized yet poorly explored genetic diversity of microalgal DGAT2s, which greatly exceeds that in higher plants (in both sequence and function, due to forces such as secondary endosymbiosis), should create copious new opportunities for lipid engineering of not just microalgae but also higher plants.

METHODS

Strains and Growth Conditions

S. cerevisiae strain H1246, which harbors knockouts of *DGA1*, *LRO1*, *ARE1*, and *ARE2* (Sandager et al., 2002), was maintained on YPD plates (1% yeast extract [w/v], 2% peptone [w/v], and 2% glucose [w/v]) solidified with 2% agar (w/v). *N. oceanica* strain IMET1 was cultivated and nitrogen deficiency induced as previously described (Moustafa et al., 2009; Li et al., 2014; Jia et al., 2015).

Gene Cloning and Phylogenetic Analysis of *NoDGAT2*s

N. oceanica DNA was synthesized and used as a template for PCR. All primers used are listed in Supplemental Table 4. PCR products were then sequenced and manually curated to obtain the full-length *NoDGAT2A-2K* protein-coding sequences (Supplemental Table 1 and Supplemental Dataset 1). In addition, extracted genome DNA was used as template to amplify the genomic *NoDGAT2* sequences that include both introns and exons. The gene structure (i.e., distributions of exons, introns, and untranslated regions) was then verified by alignment and comparison between the protein sequences and the genomic sequences.

The encoded protein sequences of known or putative *DGAT2* genes were aligned with MUSCLE version 3.8.31 (Lan et al., 2009) and further adjusted manually using BioEdit version 7.0.5.3 (Hall, 1999) before all phylogenetic analyses. The optimal substitution model of amino acid substitution was selected using the program ModelGenerator version 0.84 (Keane et al., 2006). DGAT2 from *Mycobacterium tuberculosis* was used as the outgroup.

The curated alignment was then used to construct a phylogenetic tree using the neighbor-joining (NJ) method in MEGA4.1 (Tamura et al., 2007), with the tree tested by bootstrapping with 1000 replicates. At the same time, the aforementioned multiple-sequence alignment was also used to construct the phylogenetic trees using the maximum-likelihood (ML) method via PhyML software version 3.0 (Turchetto-Zolet et al., 2011). One thousand bootstrap replicates were performed to obtain the confidence support. In the end, the phylogenesis of each NoDGAT2 was inferred via both the NJ and ML trees. Based on their consensus, the originated lineages of each *NoDGAT2* were then determined (Wang et al., 2014).

Construction of Overexpression and RNAi Vectors

For yeast, the amplified PCR products were digested with *Kpn*I and *Eco*RI for *NoDGAT2A*, *2B*, *2C*, *2D*, *2E*, *2F*, *2H*, *2I*, and *2J*, with *Bam*HI and *Eco*RI for *NoDGAT2G*, and with *Hin*dIII and *Eco*RI for *NoDGAT2K*. The products were then subcloned into pYES2 vector (Invitrogen) to form pXJ401-pXJ411 for expression in the yeast *S. cerevisiae* (see below for more details). As a positive control in yeast expression assays, the yeast *DGA1* gene encoding DGAT2 was cloned, in a manner similar to *NoDGAT2*s, to form pXJ412.

For construction of the vectors for overexpression in *N. oceanica* IMET1, *NoDGAT2A*, *2C*, and *2D* cDNA were amplified from pXJ401, pXJ403, and pXJ404 (Supplemental Table 4), respectively. *NoDGAT2*s were subcloned into pXJ004 (Supplemental Figure 13A and Supplemental Methods) to substitute *ble* gene (into *Xho*I and *Eco*RV sites). The expressing cassettes of Ptub-*NoDGAT*s-TpsbA were then amplified and subcloned into the *Hin*dIII, *Sac*II, or *Sac*I sites of pXJ015 (Supplemental Figure 13B and Supplemental Methods) to form pXJ418, pXJ420, or pXJ421, which contains *NoDGAT2A*, *2C*, or *2D*, respectively (Supplemental Figure 13C–13E).

For construction of vector for *NoDGAT2A*, *2C*, or *2D* RNAi knockdown, a 179-bp, 233-bp, or 212-bp small fragment and a 325-bp, 435-bp, or 436-bp long fragment were amplified from the *N. oceanica* IMET1 cDNA, respectively (Supplemental Table 4). The fragments were digested with *Eco*RI and *Xba*I and joined with *Xba*I sites. The joint fragments with the inverted sequences were ligated to the *Eco*RI site of the linearized phir-PtGUS vector to create phir-Pt-*NoDGAT2A*, phir-Pt-*NoDGAT2C*, or phir-Pt-*NoDGAT2D* plasmid, respectively. The promoter region of *β-tubulin* of *N. oceanica* IMET1 was amplified from genomic DNA (Supplemental Table 4), then was digested with *Sac*I and *Nco*I and ligated in the phir-Pt-*NoDGAT2A*, phir-Pt-*NoDGAT2C*, or phir-Pt-*NoDGAT2D* plasmid replacing the *P. tricornutum fcpB* promoter to form pXJ431 (with *NoDGAT2A* fragments) (Supplemental Figure 13F), pXJ433 (with *NoDGAT2C* fragments) (Supplemental Figure 13G), or pXJ434 (with *NoDGAT2D* fragments) (Supplemental Figure 13H).

Transformation of Yeasts and *N. oceanica*

Yeast mutant H1246 was transformed with an expression vector (pYES2.0) harboring coding sequence for *NoDGAT2*s using the lithium acetate procedure (Gietz and Woods, 1994), In addition, the EV pYES2.0 and the expression vector harboring the yeast *DGA1* were transformed into the mutant strain as negative and positive controls, respectively. Transformants were then selected by growth on synthetic glucose medium (2% glucose [w/v] and 0.67% yeast nitrogen base

without amino acids [w/v]) containing appropriate auxotrophic supplements (Clontech).

Nuclear transformation was performed using the linearized overexpressing vector construct and the high-voltage (11 000 V/cm) electroporation method (Wang et al., 2016). The transformant with empty pXJ015 vector was used as control. Mid-logarithmic phase algal cells (OD_{750} of 2.6) were collected for validation of successful transformants via PCR amplification of the introduced promoter and *NoDGAT2*s on the vector (Supplemental Table 4 and Supplemental Figure 14). Positive lines were then cultured for further validation of target-gene expression. For subsequent phenotyping, the transgenic lines (plus the controls, i.e., wild-type transformed with EV) were grown to OD_{750} of 4.5 ± 0.5 for 5 days, after which contents and FA profiles of both TAG and TL were tracked at 0 h, 24 h, 48 h, 72 h, and 96 h under N-depleted condition (N−) (Supplemental Methods).

Yeast Induction and PUFA Feeding

For determination of FA substrate preferences among NoDGAT2A, 2C, and 2D, supplementation of synthetic glucose cultures with LA (C18:2, n9,12), ALA (C18:3, n6,9,12), ARA (C20:4, n6,9,12,15), and EPA (C20:5, n5,8,11,14,17) was carried out with 90 μM of the appropriate FA in the presence of 0.1 g/l BSA. Cells were incubated for 20–22 h at 30°C and 150 rpm, and harvested by centrifugation.

Yeast Microsome Preparation and Non-radiolabeled DGAT *In Vitro* Assay

Yeast microsome preparation and *in vitro* assay were conducted as previously described (Liu et al., 2016a). Microsome fraction alone and microsome fraction with DAG were used as controls, and the background levels of TAG were subtracted from the data for DGAT activity analysis. The acyl-CoAs tested included palmitoyl-CoA (C16:0 CoA), hexadecenoyl-CoA (C16:1 CoA), stearoyl-CoA (C18:0 CoA), oleoyl-CoA (C18:1 CoA), linoleoyl-CoA (C18:2 CoA), α-linolenoyl-CoA (C18:3n3 CoA), γ-linolenoyl-CoA (C18:3n6 CoA), eicosatetraenoyl-CoA (C20:4 CoA), eicosapentaenoyl-CoA (C20:5 CoA), and docosahexaenoyl-CoA (C22:6 CoA); the DAGs were C16:0/C16:0, C16:1/C16:1, C18:1n9/C16:0, C16:0/C18:1, C18:1/C18:1, 1,3-C18:1/C18:1, C18:2/C18:2, and C18:3/C18:3.

Lipid Isolation and Quantification

Total lipids were extracted from dried samples using chloroform/methanol (2:1 [v/v]) with 100 mM internal control tri13:0 TAG (Sigma) and separated on a silica TLC plate using a mixture of solvents consisting of petroleum ether, ethyl ether, and acetic acid (70:30:1, by volume). To quantify the amount of TAG accumulated in yeasts expressing the *NoDGAT2* constructs, we scraped TAG bands from the TLC plate. Fatty acid methyl esters (FAMEs) were prepared by acid-catalyzed transmethylation of the TAG bands and then analyzed by GC–MS as previously described (Zhang et al., 2003). Mixed analytical standard of FAMEs (Sigma) and pentadecane (Sigma) were used as external and internal standard, respectively. The amounts of TAGs and the profiles of TAG-associated FA were calculated based on the results derived from GC–MS.

Mass Spectrometry Analysis of TAG Species

TAG species analysis was performed with an Agilent 6430 triple quadruple electrospray ionization mass spectrometer equipped with an Agilent 1290 high-performance liquid chromatograph. TAG were detected as $[M + NH_4]^+$ at the positive mode. Precursor ion and neutral loss scanning modes were employed to identify TAG species for a given class according to previously described methods (Han and Gross, 2001; Li et al., 2014; Jia et al., 2015). Fold change of the lipid content in response to N deprivation was calculated as $\log_{10}[Tc(Cx, NoDGAT2)/Tc(Cx, ScDGA1)]/[\log_{10}(|max|)]$ (Tc = content of TAG species, Cx = supplied FA) and then displayed in the heatmap. Student's *t*-test was used to compare transformant with control at the same time point. If the test gave a *p* value lower or equal to 0.05, the difference was interpreted as being significant.

Additional details on methodology are provided in Supplemental Methods.

ACCESSION NUMBERS

The GenBank Accession IDs of validated full-length sequences of the 11 *NoDGAT2*s are *2A* (KX867956), *2B* (KX867957), *2C* (KX867958), *2D* (KX867959), *2E* (KX867960), *2F* (KX867961), *2G* (KX867962), *2H* (KX867963), *2I* (KX867964), *2J* (KX867965) and *2K* (KX867955). Additional information on *N. oceanica* IMET1 genome annotation is available at http://nanno.single-cell.cn.

SUPPLEMENTAL INFORMATION

Supplemental Information is available at *Molecular Plant Online*.

FUNDING

We are grateful to support from the Natural Science Foundation of China (31425002, 31600059, 31571807, and 31401116), the Chinese Academy of Sciences (KSZD-EW-Z-017 and ZDRW-ZS-2016-3), the Natural Science Foundation of Shandong (ZR2015CQ003), the U.S. National Science Foundation (CBET-1511939), and the U.S. Office of Naval Research (N00014-15-1-2219).

AUTHOR CONTRIBUTIONS

J.X., Y.X., Q.H., Y. Li, and J.L. designed research; Y.X. performed the *ex vivo* assay in yeast; J.L. conducted the *in vitro* assay; Y.X., L.W., Q.W. and Y. Lu generated and screened overexpression lines of *N. oceanica*; Y.X., Y.-Y.L., and H.H. generated and characterized RNAi lines of *N. oceanica*; Y.X., J.J., and F.B. conducted the ESI-MS assay; Y.X. and D.W. performed phylogenetic analysis; Y.X. and J.X. analyzed gene expression data; J.X., Y.X., Y. Li, J.L., and Q.H. analyzed data and wrote the paper.

ACKNOWLEDGMENTS

No conflict of interest declared.

Received: August 24, 2017
Revised: October 17, 2017
Accepted: October 21, 2017
Published: October 26, 2017

REFERENCES

Ajjawi, I., Verruto, J., Aqui, M., Soriaga, L.B., Coppersmith, J., Kwok, K., Peach, L., Orchard, E., Kalb, R., Xu, W., et al. (2017). Lipid production in *Nannochloropsis gaditana* is doubled by decreasing expression of a single transcriptional regulator. Nat. Biotechnol. **35**:647–652.

Archibald, J.M. (2009). Secondary Endosymbiosis. Encyclopedia of Microbiology (Cambridge, MA: Academic Press), pp. 438–446.

Boyle, N.R., Page, M.D., Liu, B., Blaby, I.K., Casero, D., Kropat, J., Cokus, S.J., Hong-Hermesdorf, A., Shaw, J., Karpowicz, S.J., et al. (2012). Three acyltransferases and nitrogen-responsive regulator are implicated in nitrogen starvation-induced triacylglycerol accumulation in *Chlamydomonas*. J. Biol. Chem. **287**:15811–15825.

Chiron, H., Wilmer, J., Lucas, M.O., Nesi, N., Delseny, M., Devic, M., and Roscoe, T.J. (2015). Regulation of FATTY ACID ELONGATION1, expression in embryonic and vascular tissues of *Brassica napus*. Plant Mol. Biol. **88**:65–83.

Dolch, L.J., Rak, C., Perin, G., Tourcier, G., Broughton, R., Leterrier, M., Morosinotto, T., Tellier, F., Faure, J.D., Falconet, D., et al. (2017). A palmitic acid elongase affects eicosapentaenoic acid and plastidial monogalactosyldiacylglycerol levels in *Nannochloropsis*. Plant Physiol. **173**:742–759.

Flagel, L.E., and Wendel, J.F. (2009). Gene duplication and evolutionary novelty in plants. New Phytol. **183**:557–564.

Gee, C.W., and Niyogi, K.K. (2017). The carbonic anhydrase CAH1 is an essential component of the carbon-concentrating mechanism in *Nannochloropsis oceanica*. Proc. Natl. Acad. Sci. USA **114**:4537–4542.

Georgianna, D.R., and Mayfield, S.P. (2012). Exploiting diversity and synthetic biology for the production of algal biofuels. Nature **488**:329–335.

Gietz, R.D., and Woods, R.A. (1994). High Efficiency Transformation with Lithium Acetate. Molecular Genetics of Yeast: A Practical Approach (Cambridge, MA: Academic Press), pp. 121–134.

Guiheneuf, F., Leu, S., Zarka, A., Khozin-Goldberg, I., Khalilov, I., and Boussiba, S. (2011). Cloning and molecular characterization of a novel acyl-CoA:diacylglycerol acyltransferase 1-like gene (PtDGAT1) from the diatom *Phaeodactylum tricornutum*. FEBS J. **278**:3651–3666.

Hall, T.A. (1999). BioEdit: a user-friendly biological sequence alignment editor and analysis program for Windows 95/98/NT. Nucl. Acids Symp. Ser. **41**:95–98.

Han, X.L., and Gross, R.W. (2001). Quantitative analysis and molecular species fingerprinting of triacylglyceride molecular species directly from lipid extracts of biological samples by electrospray ionization tandem mass spectrometry. Anal. Biochem. **295**:88–100.

Horn, P.J., and Benning, C. (2016). The plant lipidome in human and environmental health. Science **353**:1228–1232.

Hu, J.Q., Wang, D.M., Li, J., Jing, G.C., Ning, K., and Xu, J. (2014). Genome-wide identification of transcription factors and transcription-factor binding sites in oleaginous microalgae Nannochloropsis. Sci. Rep. **4**:5454.

Hu, Q., Sommerfeld, M., Jarvis, E., Ghirardi, M., Posewitz, M., Seibert, M., and Darzins, A. (2008). Microalgal triacylglycerols as feedstocks for biofuel production: perspectives and advances. Plant J. **54**:621–639.

Iskandarov, U., Khozin-Goldberg, I., and Cohen, Z. (2010). Identification and characterization of Delta12, Delta6, and Delta5 desaturases from the green microalga *Parietochloris incisa*. Lipids **45**:519.

Jia, J., Han, D.X., Gerken, H.G., Li, Y.T., Sommerfeld, M., Hu, Q., and Xu, J. (2015). Molecular mechanisms for photosynthetic carbon partitioning into storage neutral lipids in *Nannochloropsis oceanica* under nitrogen-depletion conditions. Algal Res. **7**:66–77.

Keane, T.M., Creevey, C.J., Pentony, M.M., Naughton, T.J., and McInerney, J.O. (2006). Assessment of methods for amino acid matrix selection and their use on empirical data shows that ad hoc assumptions for choice of matrix are not justified. BMC Evol. Biol. **6**:29.

Klaitong, P., Fa-Aroonsawat, S., and Chungjatupornchai, W. (2017). Accelerated triacylglycerol production and altered fatty acid composition in oleaginous microalga *Neochloris oleoabundans* by overexpression of diacylglycerol acyltransferase 2. Microb. Cell Fact. **16**:61.

Knothe, G. (2008). "Designer" bodiesel: optimizing fatty ester composition to improve fuel properties. Energy Fuels **22**:1358–1364.

Kwak, S.M., Myung, S.K., Lee, Y.J., and Seo, H.G. (2012). Efficacy of omega-3 fatty acid supplements (eicosapentaenoic acid and docosahexaenoic acid) in the secondary prevention of cardiovascular disease a meta-analysis of randomized, double-blind, placebo-controlled trials. Arch. Intern. Med. **172**:686–694.

Lan, T., Yang, Z.L., Yang, X., Liu, Y.J., Wang, X.R., and Zeng, Q.Y. (2009). Extensive functional diversification of the *Populus* glutathione S-transferase supergene family. Plant Cell. **21**:3749–3766.

Lee, J.M., Lee, H., Kang, S., and Park, W.J. (2016). Fatty acid desaturases, polyunsaturated fatty acid regulation, and biotechnological advances. Nutrients **8**:23.

Li, D.W., Cen, S.Y., Liu, Y.H., Balamurugan, S., Zheng, X.Y., Alimujiang, A., Yang, W.D., Liu, J.S., and Li, H.Y. (2016). A type 2 diacylglycerol acyltransferase accelerates the triacylglycerol biosynthesis in heterokont oleaginous microalga *Nannochloropsis oceanica*. J. Biotechnol. **229**:65–71.

Li, J., Han, D., Wang, D., Ning, K., Jia, J., Wei, L., Jing, X., Huang, S., Chen, J., Li, Y., et al. (2014). Choreography of transcriptomes and lipidomes of *Nannochloropsis* reveals the mechanisms of oil synthesis in microalgae. Plant Cell. **26**:1645–1665.

Liu, J., Lee, Y.Y., Mao, X.M., and Li, Y.T. (2016a). A simple and reproducible non-radiolabeled in vitro assay for recombinant acyltransferases involved in triacylglycerol biosynthesis. J. Appl. Phycol. **29**:323–333.

Liu, J., Han, D.X., Yoon, K., Hu, Q., and Li, Y.T. (2016b). Characterization of type 2 diacylglycerol acyltransferases in *Chlamydomonas reinhardtii* reveals their distinct substrate specificities and functions in triacylglycerol biosynthesis. Plant J. **86**:3–19.

Moustafa, A., Beszteri, B., Maier, U.G., Bowler, C., Valentin, K., and Bhattacharya, D. (2009). Genomic footprints of a cryptic plastid endosymbiosis in diatoms. Science **324**:1724–1726.

Poliner, E., Pulman, J.A., Zienkiewicz, K., Childs, K., Benning, C., and Farré, E.M. (2017). A toolkit for *Nannochloropsis oceanica* CCMP1779 enables gene stacking and genetic engineering of the eicosapentaenoic acid pathway for enhanced long-chain polyunsaturated fatty acid production. Plant Biotechnol. J. https://doi.org/10.1111/pbi.12772.

Radakovits, R., Jinkerson, R.E., Fuerstenberg, S.I., Tae, H., Settlage, R.E., Boore, J.L., and Posewitz, M.C. (2012). Draft genome sequence and genetic transformation of the oleaginous alga *Nannochloropsis gaditana*. Nat. Commun. **3**:686.

Ramos, M.J., Fernandez, C.M., Casas, A., Rodriguez, L., and Perez, A. (2009). Influence of fatty acid composition of raw materials on biodiesel properties. Bioresour. Technol. **100**:261–268.

Sandager, L., Gustavsson, M.H., Stahl, U., Dahlqvist, A., Wiberg, E., Banas, A., Lenman, M., Ronne, H., and Stymne, S. (2002). Storage lipid synthesis is non-essential in yeast. J. Biol. Chem. **277**:6478–6482.

Sanjaya, Miller, R., Durrett, T.P., Kosma, D.K., Lydic, T.A., Muthan, B., Koo, A.J., Bukhman, Y.V., Reid, G.E., Howe, G.A., et al. (2013). Altered lipid composition and enhanced nutritional value of *Arabidopsis* leaves following introduction of an algal diacylglycerol acyltransferase 2. Plant Cell. **25**:677–693.

Shockey, J.M., Gidda, S.K., Chapital, D.C., Kuan, J.C., Dhanoa, P.K., Bland, J.M., Rothstein, S.J., Mullen, R.T., and Dyer, J.M. (2006). Tung tree DGAT1 and DGAT2 have nonredundant functions in triacylglycerol biosynthesis and are localized to different subdomains of the endoplasmic reticulum. Plant Cell. **18**:2294–2313.

Shoji, T., and Hashimoto, T. (2011). Recruitment of a duplicated primary metabolism gene into the nicotine biosynthesis regulon in tobacco. Plant J. **67**:949–959.

Smanski, M.J., Zhou, H., Claesen, J., Shen, B., Fischbach, M.A., and Voigt, C.A. (2016). Synthetic biology to access and expand nature's chemical diversity. Nat. Rev. Microbiol. **14**:135–149.

Tamura, K., Dudley, J., Nei, M., and Kumar, S. (2007). MEGA4: molecular evolutionary genetics analysis (MEGA) software version 4.0. Mol. Biol. Evol. **24**:1596–1599.

Timmis, J.N., Ayliffe, M.A., Huang, C.Y., and Martin, W. (2004). Endosymbiotic gene transfer: organelle genomes forge eukaryotic chromosomes. Nat. Rev. Genet. **5**:123–135.

Tonon, T., Sayanova, O., Michaelson, L.V., Qing, R., Harvey, D., Larson, T.R., Li, Y., Napier, J.A., and Graham, I.A. (2005). Fatty acid desaturases from the microalga *Thalassiosira pseudonana*. FEBS J. **272**:3401–3412.

Turchetto-Zolet, A.C., Maraschin, F.S., de Morais, G.L., Cagliari, A., Andrade, C.M.B., Margis-Pinheiro, M., and Margis, R. (2011). Evolutionary view of acyl-CoA diacylglycerol acyltransferase (DGAT), a key enzyme in neutral lipid biosynthesis. BMC Evol. Biol. **11**:263.

Vieler, A., Wu, G., Tsai, C.H., Bullard, B., Cornish, A.J., Harvey, C., Reca, I.B., Thornburg, C., Achawanantakun, R., Buehl, C.J., et al. (2012). Genome, functional gene annotation, and nuclear transformation of the heterokont oleaginous alga *Nannochloropsis oceanica* CCMP1779. PLoS Genet. **8**:e1003064.

Wang, D.M., Lu, Y.D., Huang, H., and Xu, J. (2011). Establishing oleaginous microalgae research models for consolidated bioprocessing of solar energy. Adv. Biochem. Eng. Biotechnol. **128**:69–84.

Wang, D.M., Ning, K., Li, J., Hu, J., Han, D., Wang, H., Zeng, X., Jing, X., Zhou, Q., Su, X., et al. (2014). *Nannochloropsis* genomes reveal evolution of microalgal oleaginous traits. PLoS Genet. **10**:e1004094.

Wang, Q.T., Lu, Y.D., Xin, Y., Wei, L., Huang, S., and Xu, J. (2016). Genome editing of model oleaginous microalgae *Nannochloropsis* spp. by CRISPR/Cas9. Plant J. **88**:1071–1081.

Wei, H.H., Shi, Y., Ma, X.N., Pan, Y.F., Hu, H.H., Li, Y.T., Luo, M., Gerken, H., and Liu, J. (2017a). A type-I diacylglycerol acyltransferase modulates triacylglycerol biosynthesis and fatty acid composition in the oleaginous microalga, *Nannochloropsis oceanica*. Biotechnol. Biofuels **10**:174.

Wei, L., Xin, Y., Wang, Q.T., Yang, J., Hu, H.H., and Xu, J. (2017b). RNAi-based targeted gene knockdown in the model oleaginous microalgae *Nannochloropsis oceanica*. Plant J. **89**:1236–1250.

Wijffels, R.H., and Barbosa, M.J. (2010). An outlook on microalgal biofuels. Science **329**:796–799.

Yu, S.Y., Li, H., Tong, M., Quyang, L.L., and Zhou, Z.G. (2012). Identification of a Δ6 fatty acid elongase gene for arachidonic acid biosynthesis localized to the endoplasmic reticulum in the green microalga *Myrmecia incisa* Reisigl. Gene **493**:219–227.

Zhang, Q., Chieu, H.K., Low, C.P., Zhang, S.C., Heng, C.K., and Yang, H.Y. (2003). *Schizosaccharomyces pombe* cells deficient in triacylglycerols synthesis undergo apoptosis upon entry into the stationary phase. J. Biol. Chem. **278**:47145–47155.

Zienkiewicz, K., Zienkiewicz, A., Poliner, E., Du, Z.Y., Vollheyde, K., Herrfurth, C., Marmon, S., Farré, E.M., Feussner, I., and Benning, C. (2017). *Nannochloropsis*, a rich source of diacylglycerol acyltransferases for engineering of triacylglycerol content in different hosts. Biotechnol. Biofuels **10**:8.

Zimorski, V., Ku, C., Martin, W.F., and Gould, S.B. (2014). Endosymbiotic theory for organelle origins. Curr. Opin. Microbiol. **22**:38–48.